Bulletin of Mathematical Biology (2019) 81:722–758
https://doi.org/10.1007/s11538-018-0531-2

Society for Mathematical Biology

ORIGINAL ARTICLE

A Growth-Fragmentation Approach for Modeling Microtubule Dynamic Instability

Stéphane Honoré[1,2] · Florence Hubert[3] · Magali Tournus[3] · Diana White[4]

Received: 10 November 2017 / Accepted: 31 October 2018 / Published online: 27 November 2018

Abstract
Microtubules (MTs) are protein filaments found in all eukaryotic cells which are crucial for many cellular processes including cell movement, cell differentiation, and cell division. Due to their role in cell division, they are often used as targets for chemotherapy drugs used in cancer treatment. Experimental studies of MT dynamics have played an important role in the development and administration of many novel cancer drugs; however, a complete description of MT dynamics is lacking. Here, we propose a new mathematical model for MT dynamics, that can be used to study the effects of chemotherapy drugs on MT dynamics. Our model consists of a growth-fragmentation equation describing the dynamics of a length distribution of MTs, coupled with two ODEs that describe the dynamics of free GTP- and GDP-tubulin concentrations (the individual dimers that comprise of MTs). Here, we prove the well-posedness of our system and perform a numerical exploration of the influence of certain model parameters on the systems dynamics. In particular, we focus on a qualitative description for how a certain class of destabilizing drugs, the vinca alkaloids, alter MT dynamics. Through variation of certain model parameters which we know are altered by these drugs, we make comparisons between simulation results and what is observed in in vitro studies.

Keywords Growth-fragmentation model · Banach fixed point · Microtubules dynamics

Mathematics Subject Classification 45K05 · 92C37

1 Introduction

Microtubules (MTs) are dynamic protein polymers that are found in all eukaryotic cells. They are crucial for normal cell development, aiding in many cellular processes,

✉ Diana White
dtwhite@clarkson.edu

Extended author information available on the last page of the article

including cell division, cell polarization, and cell motility (Wade 2009). Due to their role in cell movement and cell division, these polymers are often used as targets for a variety of cancer chemotherapy drugs. Many experimental studies have been completed to understand MT dynamics (Bayley et al. 1989; Desai and Mitchison 1997; Kirschner and Mitchison 1984; Walker et al. 1988), and how these dynamics are altered by the addition of MT targeting drugs (Mohan et al. 2013; Mukhtar et al. 2014; Zhou and Giannakakou 2005). However, a complete understanding of such dynamics is lacking, and so the development of new theoretical models to describe MT dynamics is important.

MTs undergo a unique type of dynamics referred to as dynamic instability, which was first described by Kirschner and Mitchison (1984). This type of dynamics is unique to MT polymers, and refers to the relative slow growth of a MT, followed by very fast depolymerization. The switch from growing to shortening is referred to as a catastrophe event, whereas the switch from shortening to growth is referred to as a rescue.

MTs are composed of tubulin heterodimers, and grow through the addition of GTP-bound tubulin (guanosine triphosphate), generally from the so-called plus end of the MT, and shrink through dissociation of GDP-bound tubulin (guanosine diphosphate) at this same end (Wade 2009). The minus end of the MT is generally more stable, being capped by stabilizing proteins at the microtubule organizing center (MTOC).

As MTs grow, older GTP-tubulin dimers hydrolyze to the lower energy GDP tubulin, creating two distinct regions along the length of a MT. That is, a back end composed of GDP tubulin, and a front end composed of GTP-tubulin. This GTP region at the growing end of a MT is referred to as the "GTP-cap". Some GTP islands may persist for a long time along the GDP-microtubule lattice (Dimitrov et al. 2008; Gardner et al. 2013). Figure 1 shows the location of the GTP-cap and GTP islands on freshly polymerized microtubules revealed by the binding of EB3 which is known to sense GTP-tubulin on microtubules (Mohan et al. 2013). If a MT is growing at a rate faster than that of hydrolysis, the MT will continue to grow. However, if the rate of hydrolysis is greater than the rate of growth, the GTP-cap region will begin to shorten. If the cap region vanishes, the MT will undergo a so-called catastrophe, and enter a state of shortening (fragmentation). The microtubule will either depolymerize completely or it will be rescued at a GTP island. See Fig. 2 for a representation of the polymerization-fragmentation-recycling cycle.

Since the discovery of dynamic instability, many stochastic, computational (Hill and Chen 2002; Maly 2002; Margolin et al. 2006, 2012), and theoretical models (Dogterom and Leibler 1993; Hinow et al. 2009; White et al. 2017) have been developed to better understand this unique type of behavior. Stochastic-type models, and many computational models provide a microscopic description of dimer addition and subtraction. In the model of Hill and Chen (2002), a Monte Carlo simulation approach was used to describe dynamic instability at the extreme tip of a MT. The model, coined the "cap" model, refers to the fact that, above a critical concentration for tubulin, MTs exist in either one of two phases: capped (by the GTP-cap) or uncapped (MT completely comprised of GDP). In the capped phase, the MT grows (with a fluctuating size in cap), and in the uncapped phase the MT quickly depolymerizes. Although this model is useful at capturing the qualitative description of MT dynamic instability

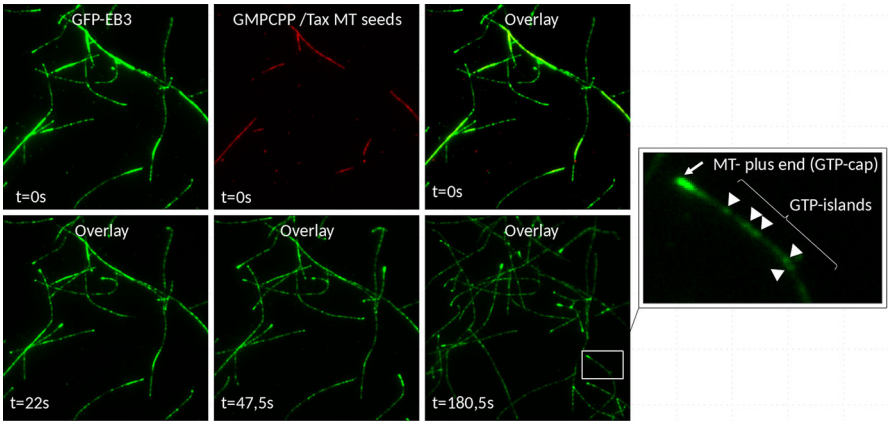

Fig. 1 In vitro plus-end tracking assay of GFP-EB3 and measurements of MT dynamics (Mohan et al. 2013). The assay was performed by growing MTs in the presence of 75 nM GFP-EB3 and 15 mM brain tubulin from GMPCPP-stabilized and paclitaxel(Tax)-stabilized MT seeds. MT seeds which were immobilized on coverslips using Poly-L-Lysine PEG-biotin streptavidin links and MT polymerization was followed by TIRF microscopy of EB3-GFP fluorescence (Color figure online)

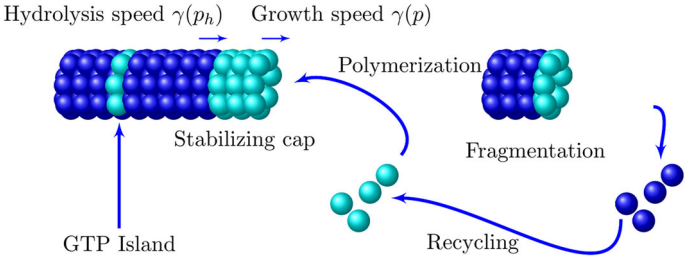

Fig. 2 Schematic representation of the polymerization-fragmentation-recycling cycle. When the hydrolysis rate exceeds the growth rate, the stabilizing cap (in light blue) gradually disappears. As soon as the cap completely vanishes, a catastrophe (shortening event) can occur: the microtubule shortens and the remaining GDP tubulin (in blue) is released into the system. GDP-tubulin is then recycled into GTP-tubulin (in light blue) which is used for the growth of other microtubules through polymerization (Color figure online)

found in experiment, it does not give a wholly accurate quantitative description. From their simulations, Hill and Chen found a critical concentration, the concentration at which MTs begin to grow, which is about one seventh of the experimental critical concentration determined by Kirschner and Mitchison (1984).

Most continuous models use advection-type terms to describe MT growth and shortening at the macroscopic level. In particular, these models keep track of the lengths of growing and shortening populations of MTs over time, where the rates of both growth and shortening are either constant (Dogterom and Leibler 1993) or depend on the free GTP-tubulin concentration (Hinow et al. 2009). In the model of Dogterom and Leibler (1993), switching between growth and shortening is described by the so-called "catastrophe" and "rescue" frequencies associated with MTs. In particular, these values must be known in advance (they are model inputs) to describe MT dynamics. In the models of Hinow et al. (2009) and White et al. (2017), these frequencies are

calculated after model simulation, which allows for a more robust examination of how these frequencies depend on MT growth dynamics.

Here, based on the Hinow model (Hinow et al. 2009), we develop a novel deterministic modeling approach in a continuous setting to describe MT dynamics. Similar to the Hinow model, we follow the mean behavior of a family of microtubules, keeping track of MT length distributions. The uniqueness of our approach is the use of a fragmentation term in the MT dynamics equation to account for sudden MT shortening, an approach that was also used by White et al. (2017). This description allows for the almost "instantaneous" shortening (catastrophe) events that are often observed in MT systems. The difference between the approach described in this paper and the approach in White et al. (2017) is that here we do not account for the MT cap length. This was accounted for in White et al. (2017) since we were exploring the effects of end-binding proteins (EBs) on MT cap dynamics. Incorporating the MT cap makes the model considerably less tractable to prove a well posedness result, and since we are not incorporating EBs into this model, we simplify this new model by removing MT cap dynamics [see the Appendix for a comparison between the model described here and that found in White et al. (2017)].

The growth-fragmentation equation is coupled to a system of ODEs that describe the dynamics of free-GTP and GDP-tubulin populations. Models consisting of an ODE coupled with an integro-partial differential equation (PDE) are already extensively used and studied in the description of Prion dynamics (Greer et al. 2006). One specificity of our model is the fragmentation kernel which is not self-similar, so that our system cannot be easily reduced to a system of ODEs, like was done for Prion. Also, similar integro-PDE type models have been used by White et al. (2014, 2015) to describe dynamic interactions between MTs and motor proteins. In particular, these models describe MT spatial patterning, which can be driven by motor proteins whose main action is to reorient the MT network.

In addition to modeling MT dynamic instability in the base case (the case without introduction of drugs), we account for the action of MT targeting agents (MTAs) on MT dynamics through variation of certain model parameters. The two major families of drugs that are used extensively as chemotherapeutic agents are the vinca alkaloids and the taxanes (Mohan et al. 2013; Zhou and Giannakakou 2005). In general, such drugs work by acting on MTs during cell division, causing cells to die (Mohan et al. 2013; Mukhtar et al. 2014; Zhou and Giannakakou 2005). MTA action on MTs can be very different in vitro and in vivo, and depends heavily on cellular/experimental conditions. As such, we will focus on qualitatively describing the in vitro action of MTAs on MT dynamics. In vitro, and at moderate to high doses, these drugs alter the dynamics of MTs by either promoting MT assembly/stabilization (MT stabilizing drugs like those of the taxane family) or promoting MT disassembly (MT destabilizing drugs like those from the vinca alkaloid family). At low (non-cytotoxic) doses, such drugs can alter MT dynamics without significantly altering the total MT polymer mass (Zhou and Giannakakou 2005). In this paper, we will primarily focus on the action of destabilizing vinblastine, as there are a number of experimental studies that describe vinblastine's role in alteration of MT dynamics (Dhamodharan et al. 1995; Jordan and Wilson 2004).

The outline of the paper is the following: In Sect. 2, we detail the development of our model which consists of an integro-partial differential equation, endowed with biologically realistic boundary conditions to describe MT dynamics, coupled with two ODEs that describe the time evolution of free GTP and GDP-tubulin concentrations. Here, we provide specific properties that certain model functions and parameters must satisfy. Section 3 is devoted to the well-posedness of the model. Here, we place more general assumptions on model parameters and functions. Finally, in Sect. 4, we perform numerical simulations to illustrate the behavior of our model in the base case. Parameters are estimated so that certain outputs of the model fit experimental data. In this section we also incorporate the action of MT targeting drugs through alteration of certain model parameters. Using these results, we explore how drugs might work to alter the normal (base-case) behavior of the MT/tubulin system.

2 Description of the Model

The evolution of the density $u(x,t)$ of microtubules of length $x \geq 0$ at time $t > 0$ is described by the one-dimensional growth-fragmentation Eq. (1). We neglect the complex cylindrical shape of MTs, and assume that they have linear structures.

$$\frac{\partial u(x,t)}{\partial t} + \gamma(p(t))\frac{\partial u(x,t)}{\partial x} = \beta(p(t))\left(-\int_0^x k(x,y)\mathrm{d}y\, u(x,t) + \int_x^\infty k(y,x)u(y,t)\mathrm{d}y\right) + N(p(t))\xi(x) \tag{1}$$

Equation (1) is coupled with a system of two ODEs, describing the time evolution of the concentrations of GTP-tubulin $p(t)$ and GDP-tubulin $q(t)$, respectively,

$$\frac{\mathrm{d}p}{\mathrm{d}t}(t) = -\gamma(p(t))\int_0^\infty u(x,t)\mathrm{d}x - N(p(t)) + \kappa q(t), \tag{2}$$

$$\frac{\mathrm{d}q}{\mathrm{d}t}(t) = \beta(p(t))\int_0^\infty u(y,t)\int_0^y (y-x)k(y,x)\mathrm{d}x\mathrm{d}y - \kappa q(t), \tag{3}$$

endowed with initial conditions $u(x,0) = 0$, $q(0) = 0$, and $p(0) = p_0 > 0$, and with the boundary condition $u(0,t) = 0$.

Equation (1) describes the three main dynamic properties of MTs: nucleation, growth and shortening. The transport term of Eq. (1) describes the growth of MTs at rate $\gamma(p)$ which depends on the free GTP-tubulin concentration, since experiments suggest that MTs undergo periods of growth that are dependent on this concentration. An example of $\gamma(p)$, which is similar to growth curves found in experiment (Lodish et al. 2000), is given by formula (4)

$$\gamma(p) = \begin{cases} 0 & \text{for} p < p_c \\ \alpha(p - p_c) & \text{for } p_c < p < p_\infty, \\ \alpha(p_\infty - p_c) & \text{for } p_\infty < p, \end{cases} \tag{4}$$

where p_c represents the critical concentration of tubulin required to initiate MT growth, p_∞ the saturation polymer concentration, and the growth rate parameter $\alpha > 0$.

The main novelty of the model is the assumption that depolymerization occurs instantaneously, and not at a finite rate. We assume this since MTs have been shown to shorten at rates that are orders of magnitude larger than rates of growth (Walker et al. 1988). The integral term of Eq. (1) describes a shortening event. We consider that such an event has a chance to occur when the fixed rate of hydrolysis γ^h exceeds the rate of growth $\gamma(p(t))$ of a MT, where we call this value p_h. In general, when the hydrolysis rate exceeds that of growth, the MT cap shortens and a catastrophe occurs only when the cap disappears. However, if we assume that the cap is sufficiently small relative to the length of a MT, such a simplifying assumption is valid.

We assume p_∞ large enough so that $\alpha(p_\infty - p_c) > \gamma^h$, and then, $\gamma(p) < \gamma^h \Leftrightarrow p < p_h$, where we define p_h as:

$$p_h = \frac{\gamma^h + \alpha p_c}{\alpha}. \tag{5}$$

If p falls below the value p_h, MTs will have a chance to shorten. However, if p stays above the value p_h, there is no MT shortening. We introduce the parameter $\beta(p)$ defined as

$$\beta(p) = \beta_\infty(1 - H(p, p_h)), \quad H(p, p_h) = \frac{1}{2}\left(1 + \tanh\left(\frac{p - p_h}{\varepsilon}\right)\right), \tag{6}$$

where β_∞ denotes the maximal shortening rate of MTs and $H(p, p_h)$ is a smooth approximation to a heavy-side function. Here, ε describes the steepness of the transition between 0 and β_∞ (i.e., the smaller the value of ε, the steeper the transition). The fact that the function β is smooth is a technical assumption that we need in Sect. 3.

The function $k(y, x)$ from Eq. (1) represents the rescaled probability that a MT of size y shortens to a MT of size $x < y$, where the remainder of the MT completely depolymerizes into GDP-tubulin dimers. Biological observations (see Fig. 3) of such shortening events point out two different cases: either MTs of length y shorten by an average fixed length x_0 and then give rise to a newborn MT of average length $y - x_0$, or MTs of length y shorten to give rise to newborn MTs of average fixed size x_1. These two cases help define the following two shortening kernels, k_0 and k_1, respectively:

$$\begin{aligned} &k_0(y, x) = G(y - x; x_0), \quad k_1(y, x) = G(x; x_1), \\ &G(z; x_*) = \frac{1}{\sigma\sqrt{2\pi}} \exp\frac{-(z - x_*)^2}{2\sigma^2}, \quad x_* > 0,\ \sigma > 0. \end{aligned} \tag{7}$$

For simplicity, we will suppress the dependence in x_* in the notation G.

In Fig. 3 (left), we show multiple kymographs from the experiment shown in Fig. 1, illustrating the dynamics of single MTs over time. A kymograph describes the growth trajectory of a single MT, and is read from top to bottom. From Fig. 3, we can observe that all MTs shorten by approximately the same distance x_0, or toward a stable part of the MT lattice (i.e., the MT seed or GTP island). Thus, the shortening kernels k_0

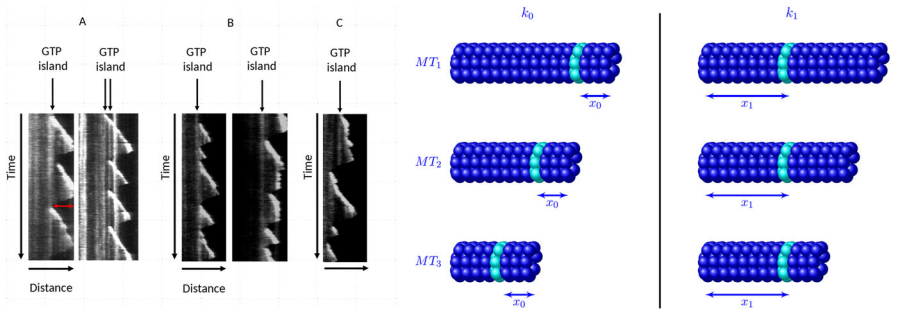

Fig. 3 Examples of the growth-fragmentation process during microtubule dynamic instability. Left: **a** Kymographs showing a MT that shortens by approximately the same size x_0 (the appropriate kernel is k_0), **b** kymographs showing a MT that shortens to the same MT size x_1 (the appropriate kernel is k_1) represented by the most distal GTP island, **c** kymograph showing that the last distal MT island is not always a rescue site. All kymographs taken from the experiment shown in Fig. 1. Right: Schematic representation of the two types of kernels, k_0 and k_1, respectively (Color figure online)

and k_1 may represent most cases, even if the reality may be more complex. Here, the shortening distances can be fit to a Gaussian like k_0, where the standard deviation σ is very small. Possible values for x_0 and its standard deviation σ are summarized in Table 1.

The final source term in Eq. (1), $N(p)$, describes MT nucleation (the birth of a MT). We assume

$$N(p) = \mu p^m H(p, p_N), \tag{8}$$

where $H(p, p_N)$ is defined as in Eq. (6). In particular, Eq. (8) states that if the value for GTP-tubulin p falls below the critical nucleation value p_N, nucleation is *switched off*. Here, μ is called the nucleation parameter and m is linked to the minimum number of GTP-tubulin dimers required for nucleation. Freshly nucleated MTs have a size between 0 and $x_{\min}$. The weight $\xi(x)$ is then defined as

$$\xi(x) = C_N(1 - H(x, x_{\min})). \tag{9}$$

Here, $x_{\min}$ is defined in Table 1 and C_N is a normalization constant that ensures we have the property

$$\int_0^\infty \xi(x)\, x \mathrm{d}x = 1. \tag{10}$$

Equations (2) and (3) represent the time evolution of GTP and GDP-tubulin, respectively. The first term in Eq. (2) describes a decrease in GTP-tubulin due to MT growth, while the second term describes a decrease due to nucleation. The final term describes GDP/GTP recycling, where $\kappa > 0$ is the recycling rate of GDP to GTP. The first term in Eq. (3) describes all GDP-tubulin which comes from a shortening event, while the second term accounts for GDP/GTP recycling.

It can be shown by formal integration that the total mass of the system (1), (2), and (3) is preserved. Specifically, the total amount of tubulin in polymer and free form

does not vary with time so that

$$\frac{\mathrm{d}}{\mathrm{d}t}\left(\int_0^\infty xu(x,t)\mathrm{d}x + p(t) + q(t)\right) = 0.$$

It can also be shown that increase in the total number of MTs is only due to nucleation. That is,

$$\frac{\mathrm{d}}{\mathrm{d}t}\left(\int_0^\infty u(x,t)\mathrm{d}x\right) = N(p(t))\int_0^\infty \xi(x)\mathrm{d}x.$$

3 Well-posedness of the PDE Model

In this section of the paper, we focus on the well-posedness of the model developed in Sect. 2. To avoid cumbersome calculations, we reduce the system defined by Eqs. (1), (2), and (3) to a system of two equations. In particular, we assume that the exchange rate of GDP-tubulin to GTP-tubulin is instantaneous (assumption that is reasonable in vitro in excess of GTP or in cells in absence of alteration of ATP-production), and so we need only to consider the equations for u and p. The generalization of the results that follow, to the full system, is straightforward. The PDE model we consider is written as:

$$\frac{\partial u(x,t)}{\partial t} + \gamma(p(t))\frac{\partial u(x,t)}{\partial x} = \beta(p(t))\left(-\int_0^x k(x,y)\mathrm{d}y\, u(x,t) + \int_x^\infty k(y,x)u(y,t)\mathrm{d}y\right) + N(p(t))\xi(x), \tag{11}$$

$$\frac{\mathrm{d}p}{\mathrm{d}t}(t) = -\gamma(p(t))\int_0^\infty u(x,t)\mathrm{d}x + \beta(p(t))\int_0^\infty u(y,t)\int_0^y (y-x)k(y,x)\mathrm{d}x\mathrm{d}y - N(p(t)), \tag{12}$$

$$u(x,0) = 0, \quad u(0,t) = 0, \quad p(0) = p_0. \tag{13}$$

A similar system was introduced and developed in the context of Prion proliferation. Global existence and uniqueness of a global solution was then studied in Laurençot and Walker (2007), Simonett and Walker (2006) and Walker (2007) using semi-group theory. The main difference between our model and that studied in Laurençot and Walker (2007) and Walker (2007) are the time-dependence of the function β and the fact that the fragmentation kernel is not self-similar.

3.1 Assumptions on the Parameters

Here, we outline assumptions on model parameters required for our main result. The polymerization growth rate $\gamma(p)$ is Lipschitz and bounded so that

$$0 \le \gamma(p_1) \le \gamma_\infty, \quad |\gamma(p_1) - \gamma(p_2)| \le \alpha|p_1 - p_2|, \quad p_1, p_2 \in \mathbb{R}^+. \tag{14}$$

The nucleation density satisfies

$$\xi \in C^1(\mathbb{R}^+), \quad \int_0^\infty \xi(x)\, x\mathrm{d}x = 1, \quad \mathrm{Supp}(\xi) \subset [x_m^\xi, x_M^\xi], \quad I_\xi := \int_0^\infty \xi(x)\,\mathrm{d}x < \infty, \tag{15}$$

$$0 \leq N(p) \leq N_\infty, \quad p \in \mathbb{R}^+. \tag{16}$$

The rate of fragmentation satisfies

$$\beta \in L^\infty(\mathbb{R}^+) \cap C^1(\mathbb{R}^+), \quad 0 \leq \beta(p) \leq \beta_\infty, \quad p \in \mathbb{R}^+. \tag{17}$$

All parameters satisfy $\gamma(p) = N(p) = \beta(p) = 0$ for $p < 0$. The fragmentation rate is bounded such that

$$\int_0^y k(y,x)\mathrm{d}x = B(y), \quad B \in L^\infty(\mathbb{R}^+), \tag{18}$$

where the kernel k satisfies

$$k(x,x) = 0,\ x \in \mathbb{R}^+, \quad k(x,0) = 0,\ x \in \mathbb{R}^+, \quad k(x,y) = 0 \text{ if } x < y, \quad x, y \in \mathbb{R}^+, \tag{19}$$

and we assume the additional properties

$$\int_0^y k(y,x)(y-x)\mathrm{d}x \leq M_0 + M_1 y, \quad \int_0^y |\partial_1 k(y,x)|\,\mathrm{d}x \leq M_2, \quad \int_0^y |\partial_2 k(y,x)|\,\mathrm{d}x \leq M_3. \tag{20}$$

Two different kernels are considered for application:

$$k_0(y,x) = \begin{cases} G_0(y-x), & y > x, \\ 0, & \text{otherwise}, \end{cases} \quad k_1(y,x) = \begin{cases} G_1(x), & y > x, \\ 0, & \text{otherwise}, \end{cases} \tag{21}$$

for some $G_0, G_1 \in \mathcal{C}^1_C(0,+\infty)$. These two kernels correspond to the experimentally observed cases illustrated in Fig. 3. The kernel k_0 satisfies properties (20) with $M_1 = 0$. In the case $M_1 = 0$, the proof of existence is easier (than when $M_1 \neq 0$); thus, we treat this case independently. For any $f \in L^\infty(\mathbb{R}^+)$ we use the notation $f_\infty := \|f\|_{L^\infty(\mathbb{R}^+)}$.

3.2 Main Result

A weak solution of to the system (11) (12) is defined as a couple $(u,p) \in C(\mathbb{R}^+; L^1(\mathbb{R}^+, (1+x)\mathrm{d}x)) \times C(\mathbb{R}^+)$ such that (11) (12) is satisfied in the sense of distributions.

Theorem 1 *Under assumptions* (14), (15), (16), (17), (18) (19) *and* (20) *, there exists a unique weak solution* $(u,p) \in C(\mathbb{R}^+; L^1(\mathbb{R}^+, (1+x)dx)) \times C(\mathbb{R}^+)$ *to the system* (11) (12)*. Moreover, it satisfies for all* $T \geq 0$

$$0 \leq p(T) \leq p_0, \quad \int_{\mathbb{R}^+} u(x,T)x dx \leq p_0, \quad \text{and} \quad \int_{\mathbb{R}^+} u(x,T)dx \leq N(p_0)T,$$
$$\text{and} \quad \int_{\mathbb{R}^+} \left|\frac{\partial u}{\partial x}(x,T)\right| dx \leq K_1 T + K_2 T^2,$$

for some positive constants K_1 and K_2 given by

$$K_1 = (x_M^\xi - x_m^\xi)N(p_0)\xi'_\infty, \quad K_2 = \frac{\beta(p_0)}{2}N(p_0)I_\xi(M_2 + M_3).$$

Strategy of the proof We build a sequence $T_0, T_1, T_2 \ldots$ and prove by induction that the system (11) (12) admits a unique solution over $[0, T_n]$, and that $T_n \to \infty$. To do so, we assume that there exists a unique solution (u^*, p^*) to the system (11), (12) over $[0, T_n]$. To extend this solution to $[T_n, T_{n+1}]$, we use the Banach fixed point theorem in the Banach space $Y = C([T_n, T])$ endowed with $\|p\|_Y = \sup_{T_n \le t \le T} \|p(t)\|$. For a given function $\bar{p} \in Y$, we define u as the unique solution for $t \ge T_n$ and $x \ge 0$ to the equation

$$\frac{\partial u(x,t)}{\partial t} + \gamma(\bar{p}(t))\frac{\partial u(x,t)}{\partial x} = \beta(\bar{p}(t))\left(-u(x,t)\int_0^x k(x,y)\mathrm{d}y + \int_x^\infty k(y,x)u(y,t)\mathrm{d}y\right) + N(\bar{p}(t))\xi(x), \tag{22}$$

$$u(x, T_n) = u^*(x, T_n), \quad u(0,t) = 0. \tag{23}$$

For the function u given by Eqs. (22) and (23), we then define $p := \mathbf{G}[\bar{p}]$ as the unique solution satisfying the equation

$$\frac{\mathrm{d}p}{\mathrm{d}t}(t) = -\gamma(\bar{p}(t))\int_0^\infty u(x,t)\mathrm{d}x + \beta(\bar{p}(t))\int_0^\infty u(y,t)\int_0^y (y-x)k(y,x)dxdy - N(\bar{p}(t)) \tag{24}$$

$$p(T_n) = p^*(T_n), \tag{25}$$

for $t \ge T_n$ and $x \ge 0$.

We obtain the unique extent (u, p) to the solution (u^*, p^*) of system (11) and (12), over $[T_n, T_{n+1}]$ as the unique fixed point to map $\mathbf{G}$ for p, and the unique u satisfying (22) and (23) where we replaced $\bar{p}$ by p. To make further notation less complicated, we drop the dependence in n for the space Y and the map $\mathbf{G}$. The sequence of lemmas that follow provide us with the necessary details needed to extend the solution to $[T_n, T_{n+1}]$, and provides us with an explicit expression for T_{n+1}. These steps will lead us to the desired end result, the proof of Theorem 1. As a first step, we show that $\mathbf{G}$ is well defined.

3.3 The Transport-Fragmentation Equation

For $a, b, c \in L^\infty(\mathbb{R}^+)$ and $T_n > 0$ given, we consider the transport-fragmentation equation for $x \ge 0$ and $t \ge T_n$

$$\begin{cases} \dfrac{\partial u(x,t)}{\partial t} + a(t)\dfrac{\partial u(x,t)}{\partial x} = b(t)\left(-u(x,t)\displaystyle\int_0^x k(x,y)\mathrm{d}y + \int_x^\infty k(y,x)u(y,t)\mathrm{d}y\right) + c(t)\xi(x), \\ u(x,T_n) = u^*(x,T_n), \quad x \ge 0, \quad u(0,t) = 0, \quad t \ge T_n. \end{cases} \tag{26}$$

Lemma 1 (Well-posedness of (22)) *Assume $a, b, c \in L^\infty(\mathbb{R}^+)$ with $a \geq 0$, $b \geq 0$, $c \geq 0$, then, there exists a unique solution to (26) in $\mathcal{C}([T_n, \infty), L^1(\mathbb{R}^+))$. Moreover, we have the following properties*

1. *Positivity. If $u^*(., T_n) \geq 0$, then $u(., t) \geq 0$ for $t \geq T_n$.*
2. *Compact support. If for some $M > x_M^\xi$, $supp(u^*(., T_n)) \subset [0, M + a_\infty T_n]$ (this is true for $T_n = 0$), then $supp(u(., t)) \subset [0, M + a_\infty t]$ for $t \geq T_n$.*

Proof The proof of Lemma 1 relies on a (second) fixed point argument. For any $\bar{u} \in C(\mathbb{R}^+, L^1(\mathbb{R}^+))$ such that $\bar{u} \geq 0$, a.e., we define $u := \mathbf{F}[\bar{u}]$ as the unique distributional solution $u \in C(\mathbb{R}^+; L^1(\mathbb{R}^+))$ to

$$\begin{cases} \dfrac{\partial u(x,t)}{\partial t} + a(t)\dfrac{\partial u(x,t)}{\partial x} = b(t)\left(-B(x)u(x,t) + \displaystyle\int_x^\infty k(y,x)\bar{u}(y,t)\mathrm{d}y\right) + c(t)\xi(x), \\ u(x, T_n) = u^*(x, T_n), \quad x \geq 0, \quad u(0,t) = 0, \quad t \geq T_n. \end{cases} \tag{27}$$

Step 1. The map F is well defined

Based on the method of characteristics, we explain why the map $\mathbf{F}$ is well defined. The characteristic curves are defined for all time $t \geq T_n$ as

$$\dot{Z}(t; t_0, y_0) = a(t), \quad Z(t_0; t_0, y_0) = y_0,$$

and for all $(x, t) \in \mathbb{R}^+ \times [T_n, +\infty)$, there exists a unique (x_0, t_0) such that either $t_0 = T_n$, either $x = 0$ and such that $Z(t; t_0, x_0) = x$. Let us first assume $\bar{u} \in \mathcal{C}^1(\mathbb{R}^+ \times \mathbb{R}^+)$ and $u^*(., T_n) \in \mathcal{C}^1(\mathbb{R}^+)$. The function u is a solution to (27) if and only if it satisfies the linear equation

$$\begin{aligned} \frac{\mathrm{d}}{\mathrm{d}t}u(Z(t; t_0, y_0), t) = b(t)\left(-B(Z(t; t_0, y_0))u(Z(t; t_0, y_0), t) + \int_{Z(t;t_0,y_0)}^\infty k(y, Z(t; t_0, y_0))\bar{u}(y, t)\mathrm{d}y\right) \\ +c(t)\,\xi(Z(t; t_0, y_0)). \end{aligned} \tag{28}$$

There exists a unique global solution $u(Z(t; t_0, y_0), t))$ to the linear ODE (28) since b, B, k, c and ξ are continuous and nonnegative. A regularization process (i.e., we approximate u^* and $\bar{u}$ by a sequence of C^1 functions u_k^* and $\bar{u}_k$) gives us the existence of a weak solution $u \in \mathcal{C}^1(\mathbb{R}^+, L^1(\mathbb{R}^+))$ for $\bar{u} \in \mathcal{C}^1(\mathbb{R}^+, L^1(\mathbb{R}^+))$ and $u^*(., T_n) \in L^1(\mathbb{R}^+)$. Uniqueness of u is clear since the difference of two solutions satisfies a linear transport equation with linear source term. Moreover, we have $u(x, t) \geq 0$, a.e.

Step 2. The solution u is compactly supported. Let us assume $\mathrm{supp}(u^*(., T_n)) \subset [0, M + a_\infty T_n]$ and $\mathrm{supp}(\bar{u}(., t)) \subset [0, M + a_\infty t]$ for $t \geq T_n$ for some $M > x_M^\xi$. The characteristic curve passing through a point (x, t) where $x > M + a_\infty t$ emanates from (x, T_n) where $x > M + a_\infty T_n$ (or from $(0, t_0)$ for a given $t_0 \geq 0$). On the characteristic curves emanating from the anchors (x, T_n) where $x \geq M + a_\infty T_n \geq x_M^\xi$, the solution u is constantly equal to zero (both the initial condition and source term are zero). Then, for $x > M + a_\infty t$, with $M > x_M^\xi$, we have $u(x, t) = 0$.

Step 3. The map F is a contraction We prove here that **F** is a contractive map in the Banach space

$$X = C^+([T_n, T_n + T]; L^1(\mathbb{R}^+, \mathrm{d}x)), \quad \|u\|_X = \sup_{T_n \le t \le T_n + T} \|u(t, .)\|_{L^1(\mathbb{R}^+, \mathrm{d}x)}.$$

The proof is a straightforward adaptation from Perthame (2007), p. 59. For $(\bar{u_1}, \bar{u_2}) \in X^2$, we define $(u_1, u_2) \in X^2$ as $u_1 := \mathbf{F}[\bar{u}_1]$ and $u_2 := \mathbf{F}[\bar{u}_2]$. The function $u = u_1 - u_2$ then satisfies for $\bar{u} = \bar{u_1} - \bar{u_2}$

$$\frac{\partial u(x,t)}{\partial t} + a(t)\frac{\partial u(x,t)}{\partial x} = b(t)\left(-B(x)u(x,t) + \int_x^\infty k(y,x)\bar{u}(y,t)\mathrm{d}y\right).$$

We multiply the above equation by $\mathrm{sign}(u)$, integrate over $\mathbb{R}^+$, and integrate with time to get

$$\|u\|_X \le T\ b_\infty B_\infty \|\bar{u}\|_X,$$

which means that as soon as $T < 1/(2b_\infty B_\infty)$, **F** is a strict contraction in the Banach space X and this proves the existence of a unique fixed point. We can iterate the operator on $[T_n + T, T_n + 2T], [T_n + 2T, T_n + 3T], \ldots$. since the condition on T does not depend on the iteration. With this iteration process, we have built a solution to (27) in $\mathcal{C}^+([T_n, +\infty), L^1(\mathbb{R}^+))$. Properties 1 and 2 of Lemma 1 are preserved by the map **F** and are thus true for the fixed point. □

The intermediate estimates stated in Lemmas 2 to 8 are useful to prove that the map **G** is a contraction from Y to Y.

Lemma 2 (L^1-estimate) *Assume $a, b, c \in L^\infty(\mathbb{R}^+)$. The solution to (26) satisfies for $A_1 = c_\infty I_\xi$*

$$\int_{\mathbb{R}^+} u^*(x, T_n)dx \le A_1 T_n \quad \textit{implies} \quad \int_{\mathbb{R}^+} u(x,t)dx \le A_1 t, \quad t \ge T_n.$$

Proof We integrate equation (22) over $\mathbb{R}^+$ and use the condition at $x = 0$ and the compact support property

$$\frac{\mathrm{d}}{\mathrm{d}t}\int_{\mathbb{R}^+} u(x,t)\mathrm{d}x = c(t)I_\xi \le c_\infty I_\xi, \quad t \ge T_n,$$

which directly implies Lemma 2 after a time integration.

Lemma 3 ($W^{1,1}$ estimate) *Assume $a, b, c \in L^\infty(\mathbb{R}^+)$. Then, there are some positive constants A_2 and A_3 such that if u^* satisfies the premise of Lemma 2, then the solution to (26) satisfies for $t \ge T_n$*

$$\int_{\mathbb{R}^+} \left|\frac{\partial u^*}{\partial x}\right|(x, T_n)dx \le A_2 T_n^2 + A_3 T_n \quad \textit{implies} \quad \int_{\mathbb{R}^+} \left|\frac{\partial u}{\partial x}\right|(x,t)dx \le A_2 t^2 + A_3 t,$$

with

$$A_2 = \frac{1}{2} b_\infty c_\infty I_\xi (M_2 + M_3), \quad A_3 = (x_M^\xi - x_m^\xi) c_\infty \xi'_\infty.$$

Proof Let us first differentiate Eq. (26) with respect to x (on a regularized solution):

$$\frac{\partial}{\partial t}\frac{\partial u}{\partial x}(x,t) + a(t)\frac{\partial}{\partial x}\frac{\partial u}{\partial x}(x,t) = b(t)\Big(- u(x,t)\frac{\partial}{\partial x}\int_0^x k(x,y)\mathrm{d}y - B(x)\frac{\partial u}{\partial x}(x,t) + \frac{\partial}{\partial x}\int_x^\infty k(y,x)u(y,t)\mathrm{d}y\Big) + c(t)\frac{\partial \xi}{\partial x}(x). \tag{29}$$

We notice that, thanks to (19) (20)

$$\frac{\partial}{\partial x}\int_0^x k(x,y)\mathrm{d}y = \int_0^x \partial_1 k(y,x)\mathrm{d}y, \quad \frac{\partial}{\partial x}\int_x^\infty k(y,x)u(y,t)\mathrm{d}y = \int_x^\infty \partial_2 k(y,x)u(y,t)\mathrm{d}y,$$

since $k(x,x) = 0$. We now formally multiply (29) by $\mathrm{sign}\left(\frac{\partial u}{\partial x}(x,t)\right)$ [actually, we multiply by a regularization of $\mathrm{sign}\left(\frac{\partial u}{\partial x}(x,t)\right)$ and pass to the limit—see section 3.4 of Perthame (2015) for details]. From this, we get

$$\frac{\partial}{\partial t}\left|\frac{\partial u}{\partial x}\right|(x,t) + a(t)\frac{\partial}{\partial x}\left|\frac{\partial u}{\partial x}\right|(x,t) = b(t)\Big(- B(x)\left|\frac{\partial u}{\partial x}(x,t)\right| - \mathrm{sign}\left(\frac{\partial u}{\partial x}(x,t)\right)u(x,t)\int_0^x \partial_1 k(y,x)\mathrm{d}y + \int_x^\infty \mathrm{sign}\left(\frac{\partial u}{\partial x}(x,t)\right)\partial_2 k(y,x)u(y,t)\mathrm{d}y\Big) + c(t)\mathrm{sign}\left(\frac{\partial u}{\partial x}(x,t)\right)\frac{\partial \xi}{\partial x}(x).$$

And, after integration we have

$$\frac{\mathrm{d}}{\mathrm{d}t}\int_{\mathbb{R}^+}\left|\frac{\partial u}{\partial x}(x,t)\right|\mathrm{d}x \le F_1(t) + F_2(t) + F_3(t) + F_4(t) + F_5(t),$$

where using Lemma 2 for F_3 and F_5,

$$F_2(t) = -b(t)\int_{\mathbb{R}^+} B(x)\left|\frac{\partial u}{\partial x}(x,t)\right|\mathrm{d}x \le 0,$$

$$F_3(t) \le b(t)\int_{\mathbb{R}^+}\int_0^x |\partial_1 k(y,x)||u(x,t)|\mathrm{d}y\mathrm{d}x \le b_\infty M_2 c_\infty I_\xi t,$$

$$F_5(t) \le b(t)\int_{\mathbb{R}^+}\int_x^\infty |\partial_2 k(y,x)||u(y,t)|\mathrm{d}y\mathrm{d}x \le b_\infty c_\infty I_\xi M_3 t$$

$$F_6(t) = c(t) \int_{\mathbb{R}^+} \left| \frac{\partial \xi}{\partial x}(x) \right| \mathrm{d}x \leq c_\infty (x_M^\xi - x_m^\xi) \xi'_\infty,$$

and since $u(0,t) = 0$, writing Eq. (26) at $x = 0$ gives us

$$F_1(t) = -a(t) \left| \frac{\partial u}{\partial x}(0,t) \right| = b(t) \int_0^\infty k(y,0) u(y,t) \mathrm{d}y + c(t)\xi(0) = 0.$$

In summary, we have

$$\frac{\mathrm{d}}{\mathrm{d}t} \int_{\mathbb{R}^+} \left| \frac{\partial u}{\partial x}(x,t) \right| \mathrm{d}x \leq b_\infty c_\infty I_\xi \, (M2 + M3)\, t + c_\infty (x_M^\xi - x_m^\xi) \xi'_\infty,$$

Then, integrating over $[T_n, t]$ we obtain the conclusion of Lemma 3.

Lemma 4 (L^1-stability) *For (a_1, b_1, c_1) and (a_2, b_2, c_2) two triplets of functions of $L^\infty(\mathbb{R}^+)$, if u_2^* satisfies the premise of Lemmas 2 and 3, the associated solutions u_1 and u_2 to (26) satisfy for $t \geq T_n$*

$$\int_{\mathbb{R}^+} |u(x,t)| dx \leq A_4 \|a_1 - a_2\|_\infty t^3 + (A_3 \|a_1 - a_2\|_\infty + A_5 \|b_1 - b_2\|_\infty)\, t^2 + I_\xi \|c_1 - c_2\|_\infty t$$

where

$$u = u_1 - u_2, \quad A_4 = \frac{A_2}{3}, \quad A_5 = 2 B_\infty c_\infty I_\xi.$$

Proof The difference u satisfies

$$\begin{aligned}
\frac{\partial u}{\partial t}(x,t) = & -a_1(t) \frac{\partial u}{\partial x}(x,t) + (a_2(t) - a_1(t)) \frac{\partial u_2}{\partial x}(x,t) \\
& + b_1(t) \left(-B(x) u(x,t) + \int_x^\infty k(y,x) u(y,t) \mathrm{d}y \right) \\
& + (b_1(t) - b_2(t)) \left(B(x) u_2(x,t) - \int_x^\infty k(y,x) u_2(y,t) \mathrm{d}y \right) \\
& + (c_1(t) - c_2(t)) \xi(x).
\end{aligned}$$

Multiplying by $\mathrm{sign}(u(x,t))$ we obtain

$$\begin{aligned}
\frac{\partial |u|}{\partial t}(x,t) \leq & - a_1(t) \frac{\partial |u|}{\partial x}(x,t) + |a_2(t) - a_1(t)| \left| \frac{\partial u_2}{\partial x}(x,t) \right| \\
& + b_1(t) \left(-B(x) |u(x,t)| + \int_x^\infty k(y,x) |u(y,t)| \mathrm{d}y \right) \\
& + |b_1(t) - b_2(t)| \left(B(x) |u_2(x,t)| + \int_x^\infty k(y,x) |u_2(y,t)| \mathrm{d}y \right) \\
& + |c_1(t) - c_2(t)| \xi(x).
\end{aligned}$$

Now, we integrate over $\mathbb{R}^+$ and get

$$\frac{\mathrm{d}}{\mathrm{d}t}\int_{\mathbb{R}^+}|u(x,t)|\mathrm{d}x \le |a_2(t)-a_1(t)|\int_0^\infty \left|\frac{\partial u_2}{\partial x}(x,t)\right|\mathrm{d}x + |c_1(t)-c_2(t)|I_\xi \\ + |b_1(t)-b_2(t)|\left(\int_0^\infty B(x)|u_2(x,t)|\mathrm{d}x + \int_0^\infty\int_x^\infty k(y,x)|u_2(y,t)|\mathrm{d}y\mathrm{d}x\right),$$

and so

$$\frac{\mathrm{d}}{\mathrm{d}t}\int_{\mathbb{R}^+}|u(x,t)|\mathrm{d}x \le \|a_1-a_2\|_\infty(A_2t^2+A_3t) \\ +I_\xi\|c_1-c_2\|_\infty + 2\|b_1-b_2\|_\infty B_\infty c_\infty I_\xi t.$$

Integrating over time and taking the supremum over $t \in [T_n, t]$, we arrive at the conclusion of Lemma 4.

Lemma 5 ($L^1(xdx)$ estimate—only for $M_1 \neq 0$) *Assume $a, b, c \in L^\infty(\mathbb{R}^+)$. Then, if u^* satisfies the premise of Lemma 2, the solution u to (26) satisfies*

$$\int_{\mathbb{R}^+} u^*(x,T_n)x\mathrm{d}x \le p_0 \quad \textit{implies} \quad \int_{\mathbb{R}^+} u(x,t)x\mathrm{d}x \le A_6e^{A_7(t-T_n)} + A_6'T_ne^{A_7(t-T_n)}, \quad t \ge T_n$$

with

$$A_6 = p_0 + \frac{c_\infty(b_\infty M_1 + I_\xi a_\infty + b_\infty M_0 I_\xi)}{b_\infty^2 M_1^2}, \quad A_6' = \frac{c_\infty I_\xi(b_\infty M_0 + a_\infty)}{b_\infty M_1}, \quad A_7 = b_\infty M_1.$$

Proof We multiply equation (26) by x and integrate over $\mathbb{R}^+$ to get

$$\frac{\mathrm{d}}{\mathrm{d}t}\int_{R^+} xu(x,t)\mathrm{d}x = a(t)\int_{\mathbb{R}^+}u(x,t)\mathrm{d}x + c(t) + b(t)\int_{\mathbb{R}^+}\int_0^y k(y,x)(x-y)u(y,t)\mathrm{d}x\mathrm{d}y$$

which implies

$$\frac{\mathrm{d}}{\mathrm{d}t}\int_{\mathbb{R}^+} xu(x,t)\mathrm{d}x \le a_\infty c_\infty I_\xi t + c_\infty + b_\infty\left(M_0c_\infty I_\xi t + M_1\int_{\mathbb{R}^+} xu(x,t)\mathrm{d}x\right).$$

The solutions to the ODE $g'(t) = r + st + wg(t)$ are written

$$g_C(t) = Ce^{wt} - \frac{rw+1}{w^2} - \frac{s}{w}t,$$

then, the solutions f to

$$f'(t) \le r + st + wf(t), \quad f(T_n) \le p_0,$$

satisfy for any $C \in \mathbb{R}$ (Gronwall Lemma)

$$f(t) \le g_C(t) + (f(T_n) - g_C(T_n))e^{w(t-T_n)}.$$

Thus, if we take C such as $g_C(T_n) = p_0$, i.e., $C = \left(p_0 + \frac{rw+s}{w^2}\right)e^{-wT_n} + \frac{s}{w}T_n e^{-wT_n}$ we have $f(t) \le Ce^{wt}$, which leads to Lemma 5.

Lemma 6 ($W^{1,1}(xdx)$ estimate—only for $M_1 \neq 0$) *Assume $a, b, c \in L^\infty(\mathbb{R}^+)$. If u^* satisfies the premise of Lemmas 2 and 5, and if*

$$\int_{\mathbb{R}^+} \left|\frac{\partial u^*}{\partial x}(x, T_n)\right| x dx \le A_9 T_n + A_{10}T_n^2 + A_{11}T_n^3,$$

then the solution to (26) satisfies

$$\int_{\mathbb{R}^+} \left|\frac{\partial u}{\partial x}(x,t)\right| x dx \le A_8 e^{A_7(t-T_n)} + A_9 t + A_{10}t^2 + A_{11}t^3 + A_{12}T_n e^{A_7(t-T_n)}, \quad t \ge T_n.$$

with

$$A_8 = \frac{b_\infty A_6(M_2+M_3)}{A_7}, \quad A_9 = c_\infty(x_M^\xi - x_m^\xi)x_M^\xi \xi'_\infty, \quad A_{10} = a_\infty \frac{A_3}{2},$$
$$A_{11} = a_\infty \frac{A_2}{3}, \quad A_{12} = \beta_\infty A'_6.$$

Proof Let us differentiate Eq. (26) with respect to x and multiply the result by $x\,\mathrm{sign}\left(\frac{\partial u}{\partial x}(x,t)\right)$. This gives

$$\begin{aligned}\frac{\partial}{\partial t}x\left|\frac{\partial u}{\partial x}\right|(x,t) + a(t)x\frac{\partial}{\partial x}\left|\frac{\partial u}{\partial x}\right|(x,t) = b(t)\left(-xB(x)\left|\frac{\partial u}{\partial x}(x,t)\right|\right.\\ -x\int_0^x \partial_1 k(x,y)\mathrm{d}y\,\mathrm{sign}\left(\frac{\partial u}{\partial x}(x,t)\right)u(x,t)\\ \left.+\mathrm{sign}\left(\frac{\partial u}{\partial x}(x,t)\right)x\int_x^\infty \partial_2 k(y,x)u(y,t)\mathrm{d}y\right) + c(t)\mathrm{sign}\left(\frac{\partial u}{\partial x}(x,t)\right)x\frac{\partial \xi}{\partial x}(x).\end{aligned}$$

After integration and using the same kind of estimates as those used for Lemma 3, we have and using Lemma 5,

$$\frac{\mathrm{d}}{\mathrm{d}t}\int_{\mathbb{R}^+} x\left|\frac{\partial u}{\partial x}(x,t)\right|\mathrm{d}x \le b_\infty A_6(M_2+M_3)e^{A_7 t} + a_\infty(A_2t^2 + A_3 t) + c_\infty(x_M^\xi - x_m^\xi)x_M^\xi \xi'_\infty$$

and the conclusion of Lemma 6 follows after time integration.

Lemma 7 ($L^1(xdx)$-stability—only for $M_1 \neq 0$) *For (a_1, b_1, c_1) and (a_2, b_2, c_2) two triplets of functions of $L^\infty(\mathbb{R}^+)$, the associated solutions u_1 and u_2 to (26) satisfy*

$$\int_{\mathbb{R}^+} x|u(x,t)|dx \leq A_{13}e^{A_7(t-T_n)} + A_{14}t, \quad t \geq T_n,$$

where

$$\begin{aligned} A_{13} &= \frac{1}{A_7} + \frac{v}{A_7^2} + \frac{2y}{A_7^3} + \frac{6z}{A_7^4}, \quad A_{14} = (M_1 + 2B_\infty)\|b_1 - b_2\|_\infty A_6, \\ v &= (A_3\|a_1 - a_2\|_\infty + M_0 I_\xi c_\infty \|b_1 - b_2\|_\infty + M_0 I_\xi b_\infty \|c_1 - c_2\|_\infty), \\ y &= M_0((A_2 + A_3)\|a_1 - a_2\|_\infty + A_5\|b_1 - b_2\|_\infty), \\ z &= M_0 A_4 \|a_1 - a_2\|_\infty. \end{aligned}$$

Proof We multiply the Eq. (3.3) (satisfied by u) by $x\text{sign}(u(x,t))$ and we integrate it over $\mathbb{R}^+$ so that

$$\begin{aligned} \frac{\mathrm{d}}{\mathrm{d}t}\int_{\mathbb{R}^+} x|u(x,t)|\mathrm{d}x \leq -a_1(t) & \\ \int_{\mathbb{R}^+} x\frac{\partial |u|}{\partial x}(x,t)\mathrm{d}x + |a_1(t) - a_2(t)| \int_{\mathbb{R}^+} x\left|\frac{\partial u_2}{\partial x}(x,t)\right|\mathrm{d}x & \\ + b_1(t)\int_{\mathbb{R}^+}\int_0^x (x-y)k(x,y)|u(x,t)|\mathrm{d}x + |c_1(t) - c_2(t)|\int_{\mathbb{R}^+} x\xi(x)\mathrm{d}x & \\ + (b_1(t) - b_2(t))\int_{\mathbb{R}^+}\int_0^x k(x,y)(x\text{sign}(u(x,t)) - y\text{sign}(u(y,t)))u_2(x,t)\mathrm{d}x. & \end{aligned}$$

Then,

$$\begin{aligned} \frac{\mathrm{d}}{\mathrm{d}t}\int_{\mathbb{R}^+} x|u(x,t)|\mathrm{d}x \leq \underbrace{b_\infty M_1}_{A_7} & \\ \int_{\mathbb{R}^+} x|u(x,t)|\mathrm{d}x + \|c_1 - c_2\|_\infty + t^3 M_0 A_4 \|a_1 - a_2\|_\infty & \\ + t^2 M_0((A_2 + A_3)\|a_1 - a_2\|_\infty + A_5\|b_1 - b_2\|_\infty) & \\ + t(A_3\|a_1 - a_2\|_\infty + M_0 I_\xi c_\infty \|b_1 - b_2\|_\infty + M_0 I_\xi b_\infty \|c_1 - c_2\|_\infty) & \\ + (M_1 + 2B_\infty)\|b_1 - b_2\|_\infty A_6 e^{A_7 t}, \quad t \in [T_n, T_n + T]. & \end{aligned}$$

A function satisfying $f'(t) \leq u + vt + yt^2 + zt^3 + me^{w(t-T_n)} + m'T_n e^{w(t-T_n)} + wf(t)$ with $f(T_n) = 0$ satisfies $f(t) \leq \left(\frac{1}{w} + \frac{v}{w^2} + \frac{2y}{w^3} + \frac{6z}{w^4}\right)e^{w(t-T_n)} + mt$, and we obtain Lemma 7.

Lemma 8 (A-priori estimate for the solution) *Let us assume that there exists a solution* $(u, p) \in C(\mathbb{R}^+; L^1(\mathbb{R}^+, (1+x)dx)) \times C(\mathbb{R}^+)$ *to the system* (11), (12) *with boundary conditions* (13) *for* $t \in [0, T_n]$ *for some given* $T_n \geq 0$. *Then, it satisfies*

$$0 \leq p(t) \leq p_0, \quad \int_{\mathbb{R}^+} u(x,T)x dx \leq p_0, \quad \text{and} \quad \int_{\mathbb{R}^+} u(x,T)dx \leq N(p_0)I_\xi T, \quad \text{for} \quad T \geq 0. \tag{30}$$

$$\text{and} \quad \int_{\mathbb{R}^+} \left|\frac{\partial u}{\partial x}(x,T)\right| dx \leq K_1 T + K_2 T^2, \quad \text{for} \quad T > 0, \tag{31}$$

for some positive constants K_1 *and* K_2 *given by*

$$K_1 = (x_M^\xi - x_m^\xi)N(p_0)\xi'_\infty, \quad K_2 = \frac{\beta(p_0)}{2}N(p_0)I_\xi(M_2 + M_3).$$

Proof The proof of (31) is a direct application of Lemma 3.

3.4 The Map G is a Contraction

We now show that $\mathbf{G}$ is a contractive map.

Lemma 9 (Estimate for $\|p\|_Y$) *We fix* $T_n \geq 0$. *For a couple of functions* $(\bar{p_1}, \bar{p_2}) \in Y^2$, *we define* $p_1 = \mathbf{G}[\bar{p_1}]$, $p_2 = \mathbf{G}[\bar{p_2}]$, $\bar{p} := \bar{p_1} - \bar{p_2}$ *and* $p := p_1 - p_2$, *where the initial conditions* p_1^*, p_2^*, u_1^* *and* u_2^* *are solutions to* (11), (12), (13) *over* $[0, T_n]$. *(We recall that* Y *and* $\mathbf{G}$ *depend on* T_n.*) Then we have*

1. *In the case* $M_1 = 0$,

$$\|p\|_Y \leq T\left(A_{15}(T_n+T)^3 + A_{16}(T_n+T)^2 + A_{17}(T_n+T) + A_{18}\right)\|\bar{p}\|_Y.$$

2. *In the case* $M_1 \neq 0$,

$$\|p\|_Y \leq T\left(A_{15}(T_n+T)^3 + A_{16}(T_n+T)^2 + \tilde{A}_{17}(T_n+T) + A_{18} + A_{19}e^{A_7(T_n+T)}\right)\|\bar{p}\|_Y,$$

where

$$\begin{aligned}
&A_{15} = (\beta_\infty M_0 + \gamma_\infty)A_4\alpha, \quad A_{16} = (\beta_\infty M_0 + \gamma_\infty)(A_3\alpha + A_5\beta'_\infty),\\
&A_{17} = N'_\infty I_\xi(\beta_\infty M_0 + \gamma_\infty) + N_\infty I_\xi(\alpha + \beta'_\infty M_0),\\
&\tilde{A}_{17} = A_{17} + M_1\beta_\infty A_{12}, \quad A_{18} = N'_\infty,\\
&A_{19} = M_1(\beta'_\infty A_6 + \beta_\infty A_{13}), \quad \tilde{A}_{19} = M_1\beta'_\infty A'_6.
\end{aligned}$$

Proof We denote by u_i the unique solution of (22) with $\bar{p} = \bar{p}_i$. We define $u := u_1 - u_2$. We have

$$\begin{aligned}\frac{dp}{dt}(t) =& -\gamma(\bar{p}_1(t))\int_{\mathbb{R}^+} u(x,t)\mathrm{d}x - (\gamma(\bar{p}_1(t)) - \gamma(\bar{p}_2(t)))\int_{\mathbb{R}^+} u_2(x,t)\mathrm{d}x\\ &+ \beta(\bar{p}_2(t))\int_{\mathbb{R}^+} u(y,t)\left(\int_0^y (y-x)k(y,x)\mathrm{d}x\right)\mathrm{d}y\\ &+ (\beta(\bar{p}_1(t)) - \beta(\bar{p}_2(t)))\int_{\mathbb{R}^+} u_1(y,t)\left(\int_0^y (y-x)k(y,x)\mathrm{d}x\right)\mathrm{d}y\\ &+ N(\bar{p}_1(t)) - N(\bar{p}_2(t)), \quad t \in [T_n, T_n + T],\end{aligned}$$

which after integration over $[T_n, t]$ for $t \in [T_n, T_n + T]$ gives us

$$\begin{aligned}|p_1(t) - p_2(t)| \le& \int_{T_n}^t \gamma(\bar{p}_1(s))\int_{\mathbb{R}^+} |u(x,s)|\mathrm{d}x\mathrm{d}s + \alpha\int_{T_n}^t |\bar{p}_1(s) - \bar{p}_2(s)|\int_{\mathbb{R}^+} u_2(x,s)\mathrm{d}x\mathrm{d}s\\ &+ \beta_\infty\int_{T_n}^t\int_{\mathbb{R}^+} |u(y,s)|\left(\int_0^y (y-x)k(y,x)\mathrm{d}x\right)\mathrm{d}y\\ &+ \beta'_\infty\int_{T_n}^t |\bar{p}_1(s)) - \bar{p}_2(s)|\int_{\mathbb{R}^+} |u_2(y,s)|\left(\int_0^y (y-x)k(y,x)\mathrm{d}x\right)\mathrm{d}y\mathrm{d}s\\ &+ N'_\infty\int_{T_n}^t |\bar{p}_1(s) - \bar{p}_2(s)|\mathrm{d}s, \quad t \in [T_n, T_n + T].\end{aligned}$$

We take the supremum over $[T_n, T_n + T]$ on both sides such that

$$\begin{aligned}\|p\|_Y \le T\|\bar{p}\|_Y&\left(N'_\infty + \int_{\mathbb{R}^+} (\beta'_\infty(M_0 + M_1 x) + \alpha)\sup_{t\in[T_n,T_n+T]} |u_2(x,t)|\,\mathrm{d}x\right)\\ &+ T\left(\int_{\mathbb{R}^+} (\gamma_\infty + \beta_\infty(M_0 + M_1 x))\sup_{t\in[T_n,T_n+T]} |u(x,t)|\mathrm{d}x\right).\end{aligned}$$

We now use the previous Lemmas that we apply for

$$\begin{aligned}a_\infty = \gamma_\infty, \quad b_\infty = \beta_\infty, \quad c_\infty = N_\infty, \quad \|a_1 - a_2\|_\infty = \alpha\|\bar{p}\|_Y,\\ \|b_1 - b_2\|_\infty = \beta'_\infty\|\bar{p}\|_Y, \quad \|c_1 - c_2\|_\infty = N'_\infty\|\bar{p}\|_Y.\end{aligned}$$

We distinguish two cases. First, we consider $M_1 = 0$. Using Lemma (8), we have

$$\int_{\mathbb{R}^+} u_2(x,T_n)\mathrm{d}x = \int_{\mathbb{R}^+} u_2^*(x,T_n)\mathrm{d}x \le N(p_0)I_\xi T_n,$$

so that Lemma (2) implies

$$\int_{\mathbb{R}^+} u_2(x,t)\mathrm{d}x \le N_\infty I_\xi(T_n + T), \quad t \in [T_n, T_n + T].$$

Since

$$\int_{\mathbb{R}^+} \left| \frac{\partial u_2}{\partial x}(x, T_n) \right| \mathrm{d}x = \int_{\mathbb{R}^+} \left| \frac{\partial u_2^*}{\partial x}(x, T_n) \right| \mathrm{d}x \leq K_1 T_n + K_2 T_n^2 \leq A_2 T_n^2 + A_3 T_n,$$

we can apply Lemma 4 and obtain

$$\begin{aligned} \|p\|_Y \leq T \|\bar{p}\|_Y \Big(& N'_\infty + (T_n + T)(N'_\infty I_\xi(\beta_\infty M_0 + \gamma_\infty) + N_\infty I_\xi(\alpha + \beta'_\infty M_0)) \\ & + (T_n + T)^2(\beta_\infty M_0 + \gamma_\infty)(A_3\alpha + A_5\beta'_\infty) + (T_n + T)^3(\beta_\infty M_0 + \gamma_\infty)A_4\alpha \Big) \end{aligned}$$

which leads to the conclusion of the first item of Lemma 9. For the case $M_1 \neq 0$, Lemma 8 implies that

$$\int_{\mathbb{R}^+} x u(x, T_n) \mathrm{d}x \leq p_0$$

so that we can apply Lemma 5. We also use Lemma 7 and we obtain

$$\begin{aligned} \|p\|_Y \leq T \|\bar{p}\|_Y \Big(& N'_\infty + (T_n + T)(N'_\infty I_\xi(\beta_\infty M_0 + \gamma_\infty) + N_\infty I_\xi(\alpha + \beta'_\infty M_0) + \beta_\infty M_1 A_{14}) \\ & + (T_n + T)^2(\beta_\infty M_0 + \gamma_\infty)(A_3\alpha + A_5\beta'_\infty) + (T_n + T)^3(\beta_\infty M_0 + \gamma_\infty)A_4\alpha \\ & + M_1(\beta'_\infty M_1(A_6 + A'_6 T_n) + \beta_\infty A_{13})e^{A_7 T} \Big) \end{aligned}$$

which ends the proof of Lemma 9.

The next Lemma is the last Lemma required for the proof of Theorem 1.

Lemma 10 *We can build a sequence* $T_0 = 0, T_1, \ldots, T_n, T_{n+1}, \ldots$ *such that*

1. *For all* $n \in \mathbb{N}$, *there exists a unique solution to system* (11) (12) *for* $t \in [0, T_n]$,
2. $\lim_{n\to\infty} T_n = +\infty$.

Proof Let us assume that (u^*, p^*) is a solution to system (11) (12) for $t \in [0, T_n]$. For the couple of functions $(\bar{p_1}, \bar{p_2}) \in Y^2$, we define $p_1 = \mathbf{G}[\bar{p_1}]$ and $p_2 = \mathbf{G}[\bar{p_2}]$. Lemma 9 gives us

$$\begin{aligned} \|\mathbf{G}[\bar{p_1}] - \mathbf{G}[\bar{p_2}]\|_Y \leq T \Big(& A_{15}(T_n + T)^3 + A_{16}(T_n + T)^2 + \tilde{A}_{17}(T_n + T) + A_{18} + A_{19}e^{A_7 T} \\ & + \tilde{A}_{19} T_n e^{A_7 T} \Big) \|\bar{p_1} - \bar{p_2}\|_Y, \end{aligned} \tag{32}$$

where the $A'_i s$ are those defined in Lemma 9. The map $\mathbf{G}$ is a strict contraction provided that the sum in (32) is strictly less than 1, which is implied by the fact that each of the 6 terms is strictly less than $1/6$. As a consequence, the map $\mathbf{G}$ is a strict contraction

over $[T_n, T_n + T]$ as soon as T satisfies the 5 following conditions:

$$T < \frac{1}{6A_{18}} =: G_1(T_n), \quad T < \frac{1}{6\tilde{A}_{17}\left(T_n + \frac{1}{6A_{18}}\right)} =: G_2(T_n),$$

$$T < \frac{1}{6A_{16}\left(T_n + \frac{1}{6A_{18}}\right)^2} =: G_3(T_n),$$

$$T < \frac{1}{6A_{15}\left(T_n + \frac{1}{6A_{18}}\right)^3} =: G_4(T_n), \quad T < \frac{1}{A_{19}} e^{-A_7\left(T_n + \frac{1}{6A_{18}}\right)} =: G_5(T_n),$$

$$T < \frac{1}{A_{19}T_n} e^{-A_7\left(T_n + \frac{1}{6A_{18}}\right)} =: G_6(T_n).$$

Then, the Banach fixed point theorem guarantees that we can extend the solution to $[T_n, T_n + T]$. The sequence defined by induction through

$$T_0 = 0, \quad T_{n+1} = T_n + \min\{G_1(T_n), G_2(T_n), G_3(T_n), G_4(T_n), G_5(T_n), G_6(T_n)\},$$

is diverging, since it is strictly increasing and the application $x \to x + \min\{G_1(x) + G_2(x) + G_3(x) + G_4(x) + G_5(x) + G_6(x)\}$ has no fixed point. □

4 Numerical Results

In this section, we describe results of the numerical simulation of equations (1), (2), and (3). First, we outline the numerical details of our approach. Then, we illustrate the behavior of our model by running a variety of simulations. In particular, we show how variations in certain model parameters change the qualitative and quantitative behavior of solutions. Such exploration gives us a better idea as to which parameters might be influenced by the addition of MTAs into a system of growing MTs. We focus our study on the action of vinblastine, a member of the destabilizing vinca alkaloid family. We do this since there are a number of studies which indicate how this drug might alter certain dynamics properties of MTs which we account for in our modeling framework (Dhamodharan et al. 1995; Jordan and Wilson 2004; Mohan et al. 2013). We simulate our model using a finite difference method. For the advection terms in Eq. (1), we use an upwinding approach, and an explicit Euler strategy for the ODEs (2) and (3). All integral terms are calculated using an order 0 quadrature method, adjusted to preserve tubulin at the discrete level.

Our domain is between 10 μm and 200 μm in length, where the distance between each grid point, Δx, is constant equal to 0.1 μm. This ensures that the support of $u(., t)$ stays in the numerical domain for all time. Also, we choose an appropriate time step

so that our scheme satisfies the CFL condition (Zauderer 2006). Our time step, Δt, equals 0.001 s.

4.1 Parameter Values in the Base Case

Our base-case parameters for the numerical simulations are summarized in Table 1. For some model parameters, their order of magnitude was determined from the literature. In particular, the growth parameter α and the GDP/GTP-tubulin exchange rate κ fall within the ranges of those given in Hinow et al. (2009), the hydrolysis rate is found in Flyvbjerg et al. (1996), the shortening rate β_∞ in Walker et al. (1988), and the dimer nucleation number m in Hinow et al. (2009); Sept et al. (1999). Other parameters were estimated in this paper, or selected through experimental observations of Honoré [experimental results not shown here, but experimental conditions are the same as those of Mohan et al. (2013)]. All model parameters, along with how they were selected, are summarized in Table 1.

4.2 Simulation Results in the Base Case

We first describe simulation output that can be compared with experimental data. One quantity of interest is the mean concentration of tubulin in polymerized form. This average, between $T_{\min}$ and $T_{\max}$, is defined as

$$\bar{u_{\text{tot}}} = \frac{1}{T_{\max} - T_{\min}} \int_{T_{\min}}^{T_{\max}} u_{\text{tot}}(t)\mathrm{d}t, \tag{33}$$

where tubulin in polymerized form at time t is defined as,

$$u_{\text{tot}}(t) = \int_0^\infty u(x,t)x\mathrm{d}x, \quad u_{\text{tot}}^0 = u_{\text{tot}}(0).$$

The value $T_{\min}$ is the time at which the first GTP-tubulin population begins to stabilize (we will describe this in more detail later in this section), $T_{\max}$ is the maximum time of simulation.

Similarly, we can write the mean MT growth rate as

$$\bar{\gamma} = \frac{1}{T_{\max} - T_{\min}} \int_{T_{\min}}^{T_{\max}} \gamma\left(p(t)\right)\mathrm{d}t. \tag{34}$$

This quantity allows the calibration of the growth parameter α in formula (4). The mean growth speed has been determined experimentally as $4.7 \pm 1.4\ \frac{\mu\text{m}}{\text{min}}$ using data collected from kymographs (recall Fig. 3). This is within the range recorded in Walker et al. (1988) [and close to that found in Mohan et al. (2013)]. The output of the model gives us a mean growth rate of $\bar{\gamma} = 5.2\ \frac{\mu\text{m}}{\text{min}}$.

Table 1 Table of model parameters

Model parameter	Description	Value	Source
α	Growth parameter	$2\ \frac{\mu m}{\mu M\,min}$	Within range found in Hinow et al. (2009) and Mohan et al. (2013)
γ^h	Baseline hydrolysis rate	$5\ \frac{\mu m}{min}$	Similar to that in Flyvbjerg et al. (1996)
β_∞	Shortening rate	$20 \pm 7.8\ \frac{\mu m}{min}$	Within range found in Walker et al. (1988)
x_0	Shortening distance	$1.6 \pm 1.2\ \mu m$	[This paper]
σ	Standard deviation of x_0	$0.2\,\mu m$	[This paper]
μ	Nucleation rate	$0.1\ \frac{1}{M\,min}$	[This paper]
m	Dimer nucleation number	2	Hinow et al. (2009) and Sept et al. (1999)
C_N	Normalization constant [from Eq. (9)] C_N	1/4	[Estimated using Eq. (10)]
x_{min}	Maximal size of nucleated MTs	$0.8\,\mu m$	[This paper]
κ	GDP/GTP-tubulin exchange rate	$2\ \frac{1}{min}$	Within range found in Hinow et al. (2009)
p_c	Critical growth value	$2\,\mu M$	[This paper—typically can be higher, $\approx 5\,\mu M$ Walker et al. (1988)]
p_N	Critical nucleation value	$12\,\mu M$	[This paper]
p_0	Initial GTP concentration	$15\,\mu M$	Within standard GTP concentration range Walker et al. (1988)
p_h	Critical fragmentation value	$4.5\,\mu M$	[Estimated using Eq. (5)]

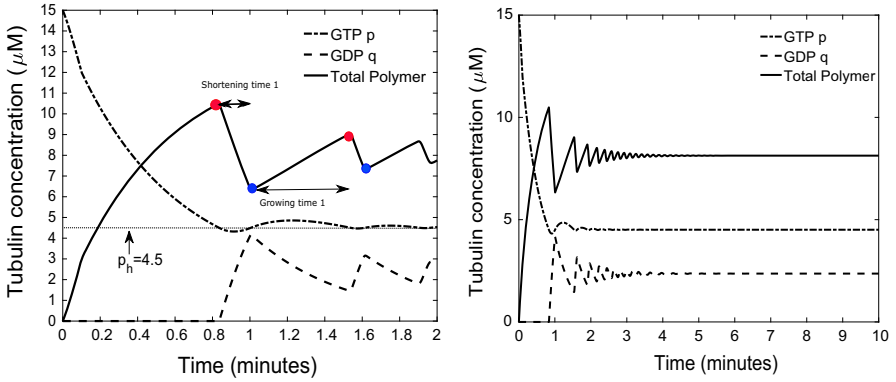

Fig. 4 Left: Example of oscillating populations of tubulin found in MTs, free GTP-tubulin, and free GDP-tubulin. Parameters used are summarized in Table 1. Shortening kernel k_0 is used. Right: Extended simulation of the figure to the left. MT dynamic instability is only sustained over a relatively short period of time. For large time, MT dynamics are completely suppressed (Color figure online)

Figures 4 (left) and (right) illustrate oscillating populations of tubulin in polymer form as well as oscillating populations of free GTP- and GDP-tubulin using the base-case model parameters given in Table 1.

In Fig. 4 (left), we show the time evolution of the three tubulin populations (GTP-tubulin p, GDP tubulin q, and tubulin in polymerized form u_{tot}) and we highlight population-level catastrophe and rescue events by red dots and blue dots, respectively. Also, examples of shortening and growing time periods are highlighted. Figure 4 (right) shows the long-time simulation (steady-state solutions) of that described on the left.

Using Fig. 4 (left), we calculate values for the mean MT length $\bar{u}_{\text{tot}}$ and growth rate $\bar{\gamma}$, using formulas (33) and (34), where $T_{\min}$ is set to T_1 (the time of the first catastrophe event). These values are given by 7.9 μM and 5.2 $\frac{\mu\text{m}}{\text{min}}$, respectively. From Fig. 4 (left), we see that at T_1 the GTP-tubulin concentration approaches a mean value which is close in value to p_{h} (4.5 μM, see Table 1).

The value of p drives the system through the nucleation rate $N(p)$, the shortening rate $\beta(p)$, and the growth rate $\gamma(p)$. Recall that, the critical nucleation value p_{N} = 12 μM, the critical growth value $p_{\text{c}} = 2\,\mu\text{M}$ and the critical fragmentation value $p_{\text{h}} = \dfrac{\gamma^{\text{h}} + \alpha p_{\text{c}}}{\alpha} = 4.5\,\mu\text{M}$. At time $t = 0$, $p = 15\,\mu\text{M}$, thus $N(p) > 0, \beta(p) = 0$ and $\gamma(p) > 0$: new microtubules are formed by nucleation and they grow so that the total mass of microtubules increases and p decreases. From Fig. 4 (left), at time $t = 0.1$ min, p goes below the critical nucleation value p_{N}; from that point, nucleation stops, which slows down the creation of polymerized tubulin. At time $t = 0.8$ min, p reaches the critical value p_{h} and fragmentation is initiated: microtubules start to shorten, and free GDP-tubulin q is created. We notice that the amplitude of the oscillations, as well as the period of oscillation, decrease with time. This result suggests that MT oscillations may be sustained over a relatively short period of time. However, at the individual level, the MT instability is still present.

4.3 Influence of β_∞ and x_* on MT Dynamics for the Two Kernels

In this section, we show simulation results for system (1), (2), and (3) for the different shortening kernels, k_0 and k_1, described in Eq. (7). First, we observe that for the range of parameters tested, the macroscopic variables $(U, u_{\text{tot}}, p, q)$, where $U(t) = \int_{\mathbb{R}} u(x,t)\mathrm{d}x$, and the MT size distribution $u(x,t)$ converge to some steady state in large time.

In both Figs. 5 and 6 we illustrate the time evolution of the macroscopic variables (u_{tot}, p, q) (bottom) and the final profile of the microscopic variable u (top) for kernels k_0 (left) and k_1 (right). As $p(t) < p_{\text{N}}$ after some time t_{N}, the quantity U is constant after this time. We consider that microscopic equilibrium is reached numerically as soon as for some t, we have the criterion $\|u(.,t) - u(.,t+dt)\|_\infty \leq 10^{-10}$ satisfied. Notice that macroscopic equilibrium is reached before microscopic equilibrium.

In Fig. 5, we explore the dependence of MT dynamics on x_*. In the range of biologically relevant parameters ($x_0 \leq 3.8\,\mu\text{m}$ and $x_1 \leq 5\,\mu\text{m}$), the macroscopic behavior does not quantitatively depend on x_*: p converges to p_{h}, and q and u_{tot} converge to some value independent of x_*. The transient behavior is qualitatively the same: the relaxation toward steady state occurs after a few oscillations. The only difference between the transient behaviors is the time at which equilibrium is reached (i.e., it strongly depends on x_*). For example, for $x_0 = 5\,\mu\text{m}$, $T_\infty \approx 60$ min and for $x_0 = 1.6\,\mu\text{m}$, $T_\infty \approx 180$ min. Differences in x_* also change the shape of the stationary profile for u. For larger values of x_* (here $x_1 \geq 10\,\mu\text{m}$ and $x_0 \geq 20\,\mu\text{m}$ (results not shown for x_0)), p can converge, in large time, to a value smaller than p_{h} and close to p_{c}.

In Fig. 6, we explore the dependence of MT dynamics on β_∞. Here again, for biologically relevant values of β_∞ ($\beta_\infty \geq 5\ \frac{\mu\text{m}}{\text{min}}$ for k_0, $\beta_\infty \geq 1\ \frac{\mu\text{m}}{\text{min}}$ for k_1), the macroscopic and microscopic equilibrium does not depend on β_∞: after damped oscillations, p converges to p_{h} and q and u_{tot} converge to some values independent of β_∞. Further, the stationary profile for u is independent of β_∞. However, for smaller values of β_∞, p converges to some $p(\beta_\infty) \neq p_{\text{h}}$, as well as q and u. In Sect. 4.5, we provide insight into how these behaviors can be predicted directly from a mathematical analysis of the system.

4.4 Dependence of p_{h} on MT Dynamics: Insight into Drug Effects

In this section, we show how variations in p_{h} change the total polymerized tubulin and GTP-tubulin concentration. We do so in order to test whether our results are consistent with what we know about how changes in this parameter (due to variations in MTA concentration) alter MT dynamics. In in vitro experiments it has been shown that high concentrations of vinblastine (Dhamodharan et al. 1995; Jordan and Wilson 2004), a member of the vinca alkaloid family, promotes MT depolymerization. However, at low doses of this drug, it suppresses MT dynamic instability. Specifically, MT growth rates and shortening rates decrease, while catastrophe is suppressed. Further, shortening lengths are also decreased. These dynamic changes result in almost constant overall polymer mass (with only minor MT depolymerization). However, in the presence of

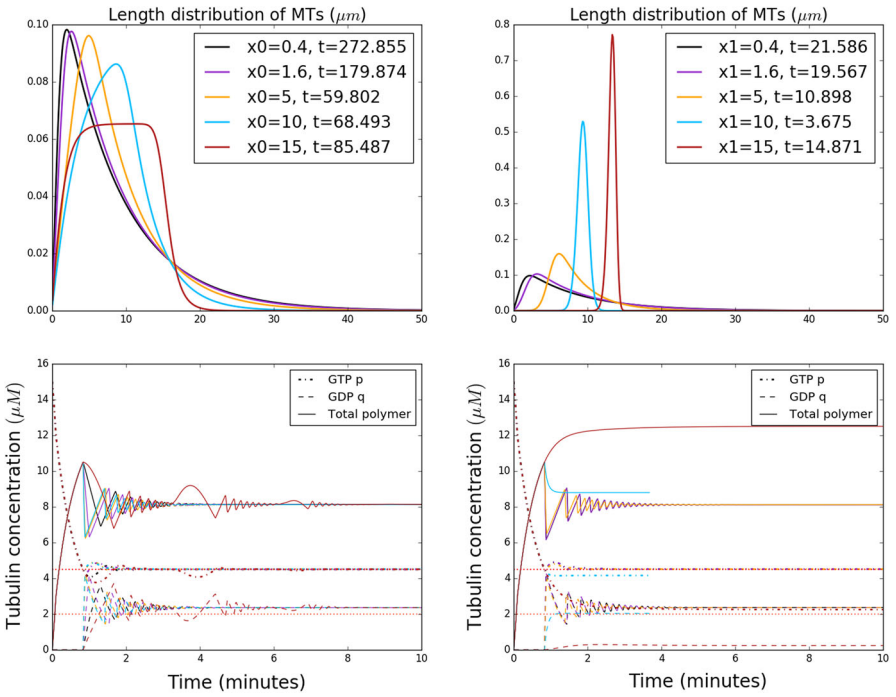

Fig. 5 Comparison of the different transient behaviors for the macroscopic variables (u_{tot}, p, q) (bottom) and asymptotic behavior for the variable u for different values of x_0 and x_1. Left: k_0, $\beta_\infty = 20$, Right: k_1, $\beta_\infty = 20$ (Color figure online)

EBs, which is the case in cells, vinblastine increases catastrophe frequency, slightly increases the MT growth rate, and decreases MT growth length (Mohan et al. 2013).

Figure 7 corresponds to simulation results for changes in the critical fragmentation value p_{h} (i.e., the hydrolysis rate) from the base-case value (see Table 1). From Fig. 7 (left), we see a decrease in tubulin in polymer form u_{tot} for increasing p_{h}. Further, we see that increases in p_{h} (from the base case) work to promote MT dynamics by increasing the number of catastrophe events. Figure 7 (right) shows the corresponding changes in the GTP-tubulin concentration. Here, it is noted that as p_{h} increases, which corresponds to an increase in the hydrolysis rate γ^{h}, the level of free GTP-tubulin in the system increases. This result makes sense, due to the fact that as a MT depolymerizes (at high values of the hydrolysis rate), free tubulin is released back into the system.

Vinblastine binds to free tubulin rapidly (and reversibly) and also binds to the extreme end of MTs (Jordan and Wilson 2004). At high concentrations, vinblastine has also been shown to bind (with low affinity) to sites along the MT surface, which is believed to help induce the peeling of protofilaments at the MT ends. These drugs bind to the vinca domain near the GTP hydrolyzable site on β-tubulin, and act on MTs (at higher concentrations) by the reducing the GTP-cap size (Mohan et al. 2013), while having little effect on the MT growth rate (this remains near constant). This phenomenon is linked to the speeding up of GTP hydrolysis, which corresponds to

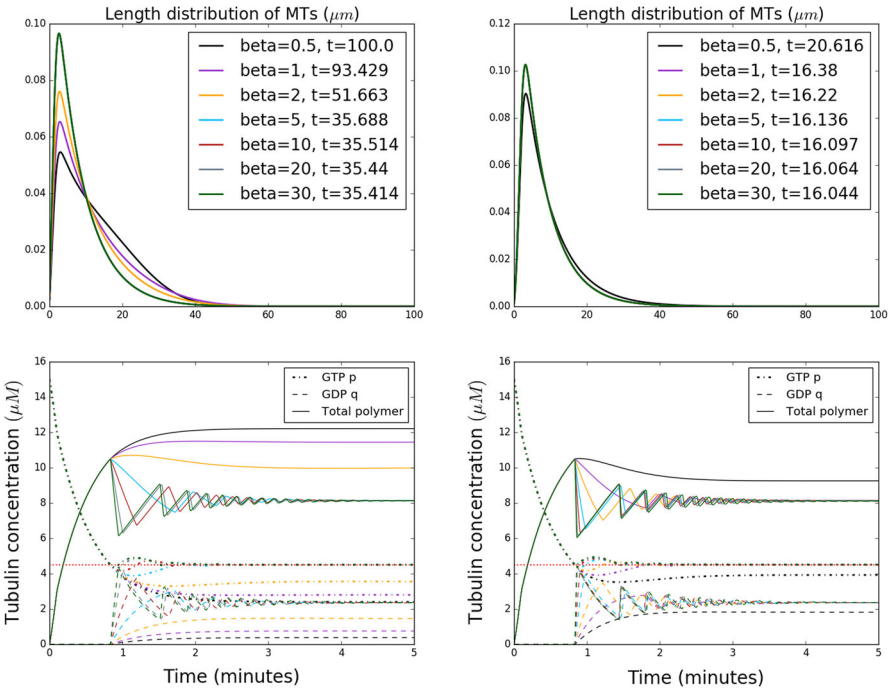

Fig. 6 Comparison of the different transient behaviors for the macroscopic variables (u_{tot}, p, q) (bottom) and asymptotic behavior for the variable u for different values of β_∞. Left: $k_0, x_0 1.6$, Right: $k_1, x_1 = 1.6$ (Color figure online)

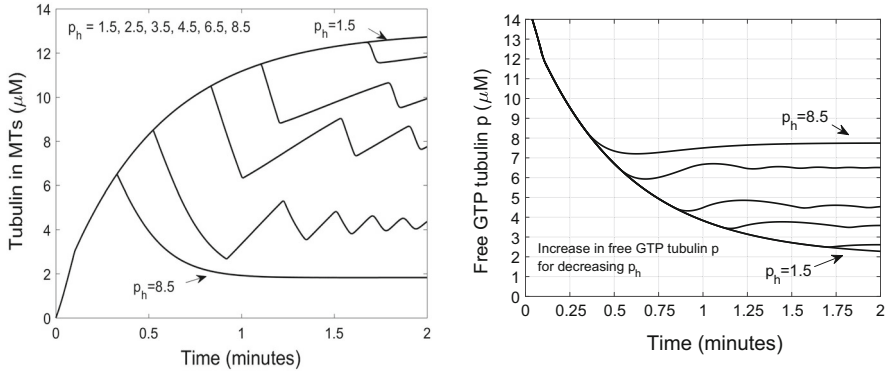

Fig. 7 Left: Changes in polymerized tubulin due to variations in the hydrolysis rate. Right: Variation of the free GDP-tubulin $p(t)$ with respect to p_{h}

an increase in p_{h} in our model. This mechanism of action is not only seen at high depolymerizing concentrations, but also at low concentrations in the presence of EBs (Mohan et al. 2013). Our results are consistent with these observations. In particular, increasing GTP hydrolysis aids in MT depolymerization (shown in Fig. 7).

4.5 Asymptotic Profile for *u* with Respect to Initial Condition

In this paragraph, we consider a fragmentation kernel of type k_0 [Eq. (21)] with $\sigma = 1$ and all the parameters given in Table 1 except for $p_\mathrm{h} = 6$ and the initial condition. All the plots displayed on Fig. 8 are obtained for $p_0 = 11,\ q_0 = 0$, and four different initial size distributions IC1: $u_0(x) = u_{5,10}(x)$, IC2: $u_0(x) = u_{5,10}(x) + u_{10,10}(x)$, IC3: $u_0(x) = u_{10,1}(x)$, IC4: $u_0(x) = u_{5,1}(x)$, where

$$u_{x_\mathrm{c},\sigma}(x) = \exp\left(-\frac{(x - x_\mathrm{c})^2}{\sigma}\right),$$

and all the initial profiles being rescaled to satisfy $\int_{\mathbb{R}^+} x u_0(x)\mathrm{d}x = 1$. The numerical results suggest that the system relaxes toward an equilibrium state, i.e., that p and q converges toward some limiting values p^* and q^*, and that the size distribution $u(x, t)$ converges toward an asymptotic profile $u^*(x)$. The limiting value for p is $p^* = p_\mathrm{h}$ and the value for q^* (see Fig. 8, upper left) and then the asymptotic profile u^* both depend on the initial distribution u_0 (see Fig. 8, upper right and Fig. 9). The initial value p_0 is small enough so that there is no nucleation at time $t = 0$, and the numerical simulations show that the value of $p(t)$ always stay below the threshold that triggers nucleation. As a consequence, the total number of polymers $U(t) = \int_{\mathbb{R}^+} u(x, t)\mathrm{d}x$ is preserved over time. The initial number of polymers is closed for IC1 and IC4 (respectively, 0.197 and 0.2), and stay close for all time. Since at the beginning of the dynamic, fragmentation is turned off (i.e., $p(t) \geq p_\mathrm{h}$, see Fig. 8, upper left) the evolution of the system (u, p, q) only depends on $p(t),\ q(t)$ and $U(t)$ (see system (1), (2), (3)) which explains why the time evolution of the macroscopic quantities for IC1 and IC4 are almost superimposed (Fig. 8, upper left).

Our guess is that the asymptotic state satisfies

$$\gamma(p_\mathrm{h})\frac{\partial u^*}{\partial x}(x) = \beta(p_\mathrm{h})\left(-\int_0^x k(x, y)\mathrm{d}y\ u^*(x) + \int_x^\infty k(y, x)u^*(y)\mathrm{d}y\right) + N(p_\mathrm{h})\xi(x), \quad (35)$$

$$\text{and } q^* = \frac{\gamma(p_\mathrm{h})}{\kappa}\int_0^{+\infty} u^*(x)\mathrm{d}x + \frac{N(p_\mathrm{h})}{\kappa}.$$

Proving that the steady state (u^*, p_h, q^*) is attractive is a difficult problem. Long-time asymptotic behavior for general growth-fragmentation equations has been described in Escobedo et al. (2005) using semi-group theory. For systems of equations, the problem is more tricky. Some work in this direction has been initiated in Calvez et al. (2010), but no proof of convergence has been shown. In the general case, due to the structure of kernels k_0 and k_1, the system can not be reduced to a closed system of ODEs in (U, p, q), as was done for similar systems (Greer et al. 2006). However, we can do this for very specific kernels, and this enables us to give insight into the qualitative asymptotic behavior we expect for the general system.

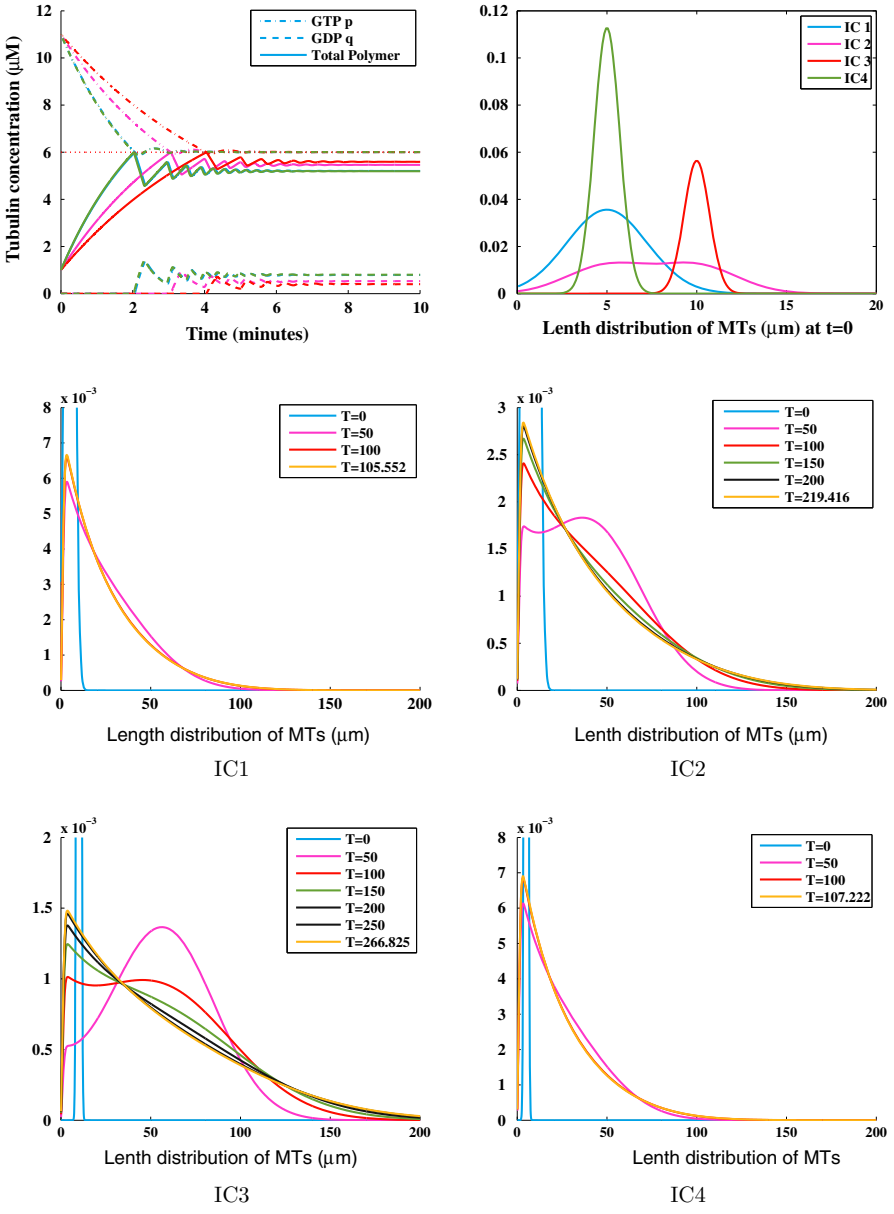

Fig. 8 Upper left: Time evolution of the macroscopic quantities $p(t), q(t)$ and the mass $\int_{\mathbb{R}+} xu(x,t)\mathrm{d}x$ for different initial size distributions u_0, IC1: cyan, IC2: pink, IC3: red and IC4: green. Upper right: Four different initial size distributions u_0. On the four other plots are drawn the time evolution of the size distribution u until it reaches equilibrium (Color figure online)

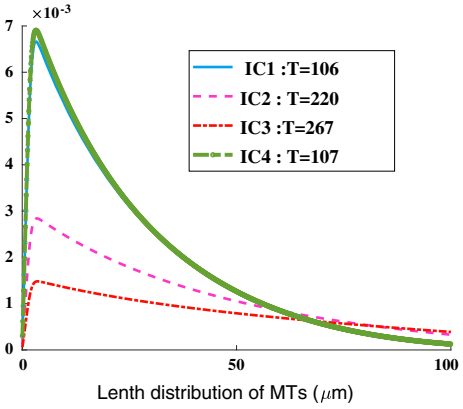

Fig. 9 Asymptotic size distribution for the microtubules, for different initial size distributions u_0 (Color figure online)

4.6 Asymptotic Behavior on a Simplified Model

A study can be performed on a simplified model, in the case of a simple island kernel $k_1(y, x) = \delta_{x_1}(x)$ for $x_1 \geq 0$.

$$\begin{cases} \dfrac{\partial u}{\partial t} + \gamma(p(t))\dfrac{\partial u}{\partial x} = \beta_\varepsilon(p(t))\left(-u(x,t)\chi_{x\geq x_1} + \delta_{x=x_1}\displaystyle\int_{x_1}^{\infty} u(y,t)\mathrm{d}y\right) + \mu H_\varepsilon(p(t), p_\mathrm{N})p(t)^2\xi(x), \\ p'(t) = -\gamma(p(t))\displaystyle\int_0^\infty u(x,t)\mathrm{d}x + \kappa q(t) - \mu H_\varepsilon(p(t), p_\mathrm{N})p(t)^2, \\ q'(t) = -\kappa q(t) + \beta_\varepsilon(p(t))\displaystyle\int_0^\infty (x - x_1)u(x,t)\mathrm{d}x, \\ u(x,0) = u_0(x), \quad u(0,t) = 0, \quad p(0) = p_0, \quad q(0) = q_0 \geq 0. \end{cases} \tag{36}$$

This type of kernel does not satisfy the technical assumptions (7) guaranteeing well-posedness of the model, since it is not a smooth function, but can be seen as a limiting case of Gaussian kernels k_1^δ centered in x_1. If we integrate the first line of (36) we obtain the closed system

$$\begin{cases} U'(t) = \mu H_\varepsilon(p(t), p_\mathrm{N})p(t)^2 I_\xi, \\ p'(t) = -\gamma(p(t))U(t) + \kappa q(t) - \mu H_\varepsilon(p(t), p_\mathrm{N})p(t)^2, \\ q'(t) = -\kappa q(t) + \beta_\varepsilon(p(t))\left(u^0_{\mathrm{tot}} + p_0 + q_0 - p(t) - q(t) - x_1 U(t)\right), \\ U(0) = U_0 \geq 0, \quad p(0) = p_0 \geq 0, \quad q(0) = q_0 \geq 0. \end{cases} \tag{37}$$

where $u^0_{\mathrm{tot}} = u_{\mathrm{tot}}(0)$.

We assume

$$H_\varepsilon(p,z) = \begin{cases} 0 & p \leq z - \varepsilon, \\ 1 & p \geq z + \varepsilon, \end{cases} \quad \frac{\partial}{\partial p}H_\varepsilon(p,z) > 0, \quad \beta_\varepsilon(p) = \beta_\infty\left(1 - H_\varepsilon(p, p_\mathrm{h})\right), \quad H_\varepsilon \in C^1(\mathbb{R}\times\mathbb{R}), \tag{38}$$

and the technical hypotheses

$$x_1 I_\xi < 1, \quad u^0_{\text{tot}} - x_1 U_0 \geq 0, \tag{39}$$

and

$$\gamma \text{ satisfies (14)}, \quad \gamma \in \mathcal{C}^\infty(\mathbb{R}^+). \tag{40}$$

Proposition 1 (Existence and uniqueness of global solutions for) *Assuming* (38), (39), *and* (40), *there exists a unique global solution to* (37)

Proof Local existence and uniqueness are guaranteed by the Cauchy Lipschitz theorem. We now prove that the maximal solution defined on $[0, T)$ for some $T > 0$ is positive and uniformly bounded with time. Since $U_0 \geq 0$, first line of (37) implies that $U(t) \geq 0$ for $t \in [0, T)$. We denote

$$w(t) = u^0_{\text{tot}} + p_0 + q_0 - p(t) - q(t) - x_1 U(t). \tag{41}$$

System (37) and assumption $x_1 I \xi < 1$ implies

$$\begin{aligned} w'(t) &= -p'(t) - q'(t) - x_1 U'(t) \\ &= \gamma(p(t))U(t) + \mu H_\varepsilon(p(t), p_{\text{N}}) p^2(t) \left(1 - x_1 I_\xi\right) \\ &\quad + \beta_\varepsilon(p(t))w(t) \geq \beta_\varepsilon(p(t)))w(t), \end{aligned} \tag{42}$$

which gives $w(t) \geq 0$ since assumption (39) implies $w(0) \geq 0$. Assume now by contradiction that there exists some $t_1 \leq T$ such that $q(t_1) < 0$. Then, since $q(0) \geq 0$, there exists $0 \leq t_0 < t_1$ such that $q(t_0) = 0$ and $q(t) \leq 0$ for $t \in [t_0, t_1]$. Then, using the mean value theorem, there is $\bar{t} \in [t_0, t_1]$ such that $q'(\bar{t}) < 0$, whereas using third line of system (37) and the non negativity of w, we have $q'(\bar{t}) = -\kappa q(\bar{t}) + \beta(p(\bar{t}))w(\bar{t}) \geq 0$, which is absurd. As a consequence, for all $t \in [0, T]$, $q(t) \geq 0$. We do the same for p, assuming again by contradiction that there exists some $t_1 \leq T$ such that $p(t_1) < 0$. Using the same argument than for q, there exists $0 \leq t_0 < t_1$ such that $p(t_0) = 0$ and $p(t) \leq 0$ for $t \in [t_0, t_1]$ and $\bar{t} \in [t_0, t_1]$ such that $p'(\bar{t}) < 0$, whereas using second line of system (37), we have $p'(\bar{t}) = -\gamma(p(\bar{t}))U(\bar{t}) + \kappa q(\bar{t}) - \mu H_\varepsilon(p(\bar{t}), p_N) p(\bar{t})^2 \geq 0$, using here that $q(\bar{t})$ is non negative. As a consequence, for all $t \in [0, T]$, $p(t) \geq 0$. In conclusion, the solution is non negative and uniformly bounded, and then the maximal solution is global.

For the next result, we assume (for simplicity) that nucleation is turned off, i.e., $\mu = 0$. This enables us to guarantee that the quantity U does not evolve with time. Note that for biological relevant datasets, simulation results correspond to a certain time t_{N}, where the function p stays below the threshold p_{N}, thus corresponding to nucleation being turned off. System (37) then becomes

$$\begin{cases} p'(t) = -\gamma(p(t))U_0 + \kappa q(t), \\ q'(t) = -\kappa q(t) + \beta_\varepsilon(p(t)) \left(u^0_{\text{tot}} + p_0 + q_0 - p(t) - q(t) - x_1 U_0\right), \\ p(0) = p_0 \geq 0, \quad q(0) = q_0 \geq 0. \end{cases} \tag{43}$$

The following proposition expresses that for ε small enough, and for x_1 larger than a threshold value $\bar{x}$, then the limiting value for p is very close to p_{h}. For x_1 smaller than the threshold value $\bar{x}$, we have the limiting value for p very close p_{h} for β_∞ larger than a threshold value $\bar{\beta}$, but for $\beta_\infty < \bar{\beta}$ it may happen that the limiting value for p is smaller than p_{h}. This is in accordance with what is observed numerically for the complete system.

Proposition 2 *Assuming* (21)*, then the system* (43) *has a unique equilibrium point* $(p_\varepsilon^*, q_\varepsilon^*)$ *on* $\mathbb{R}^+ \times \mathbb{R}^+$*, this point is asymptotically stable and satisfies*

- *if* $\beta_\infty < \bar{\beta}(x_1)$*, then* $p_\varepsilon^* \in [0,\, p_{\mathrm{h}} - \varepsilon)$*,*
- *if* $\beta_\infty \geq \bar{\beta}(x_1)$*, then* $p_\varepsilon^* \in [p_{\mathrm{h}} - \varepsilon,\, p_{\mathrm{h}} + \varepsilon]$*,*

with

$$\bar{x} = \frac{u_{\mathrm{tot}}^0 + p_0 + q_0 - (p_{\mathrm{h}} + \varepsilon)}{U_0} - \frac{\gamma(p_{\mathrm{h}} + \varepsilon)}{\kappa}, \quad \bar{\beta}(x_1) = \frac{\gamma(p_{\mathrm{h}} - \varepsilon)}{\bar{x} - x_1 + \dfrac{2\varepsilon}{U_0} + \dfrac{\gamma(p_{\mathrm{h}} + \varepsilon) - \gamma(p_{\mathrm{h}} - \varepsilon)}{\kappa}}.$$

Proof **Equilibrium.** The equilibrium points (p^*, q^*) (we omit the index ε to lighten the notations) are solutions to

$$\gamma(p^*)U_0 = \kappa q^*, \quad \kappa q^* = \beta_\varepsilon(p^*)\left(u_{\mathrm{tot}}^0 + p_0 + q_0 - p^* - q^* - x_1 U_0\right). \tag{44}$$

Then

$$q^* = \frac{\gamma(p^*)U_0}{\kappa} \tag{45}$$

and p^* necessarily satisfies $\Phi(p^*) = 0$, with

$$\Phi(p) = \beta(p)W(p) - \gamma(p)U_0, \quad W(p) = u_{\mathrm{tot}}^0 + p_0 + q_0 - p - \frac{U_0\gamma(p)}{\kappa} - x_1 U_0.$$

We first notice that $\Phi(p_{\mathrm{h}} + \varepsilon) = -\gamma(p_{\mathrm{h}} + \varepsilon)U_0 < 0$ and that for $p \geq p_{\mathrm{h}} + \varepsilon$, $\Phi'(p) = -\gamma'(p)U_0 \leq 0$, then the solutions to $\Phi(p) = 0$ belong to $[0,\, p_{\mathrm{h}} + \varepsilon)$. Also notice that $\Phi(0) = W(0) > 0$, so that Φ has at least one zero in $[0,\, p_{\mathrm{h}} + \varepsilon)$. We also notice that $W'(p) < 0$ for $p \geq 0$. We now distinguish different cases.

Case 1. $W(p_{\mathrm{h}}+\varepsilon) > 0$ *which is* $x_1 < \bar{x}$. In this case, for $p \in [0,\, p_{\mathrm{h}}+\varepsilon)$, $W(p) > 0$ and then $\Phi'(p) < 0$. Then, there exists one unique $p^* \in [0,\, p_{\mathrm{h}} + \varepsilon)$ such that $\Phi(p^*) = 0$.

Case 2. $W(p_{\mathrm{h}}+\varepsilon) \leq 0$ *which is* $x_1 \geq \bar{x}$. Then, there exists a unique $\bar{p} \in [0,\, p_{\mathrm{h}}+\varepsilon]$ such that $W(\bar{p}) = 0$, and then $\Phi(\bar{p}) < 0$. As a consequence, there exists $p^* \in [0,\, \bar{p}]$ such that $\Phi(p^*) = 0$. For $p \in [0,\, \bar{p}]$, we have $W(p) > 0$, thus $\Phi'(p) < 0$ which guarantees that there is no other solution of $\Phi(p) = 0$ for $p \in [0,\, \bar{p}]$, and for $p \in [\bar{p},\, p_{\mathrm{h}} + \varepsilon]$, we have $\Phi(p) < 0$, which guarantees that there is no other solution of $\Phi(p) = 0$ for $p \in [\bar{p},\, p_{\mathrm{h}} + \varepsilon]$. In both cases 1 and 2, depending on the sign of $\Phi(p_{\mathrm{h}} - \varepsilon)$, we give finer estimates on p^*.

Sub-case a. $\Phi(p_{\mathrm{h}} - \varepsilon) < 0$ *which is* $\beta_\infty < \bar{\beta}(x_1)$. Here, the unique solution p^* lies in $[0,\, p_{\mathrm{h}} - \varepsilon)$.

Sub-case b. $\Phi(p_h - \varepsilon) \geq 0$ *which is* $\beta_\infty \geq \bar{\beta}(x_1)$. Now, the the unique solution p^* lies in $[p_h - \varepsilon, p_h + \varepsilon]$.

Stability. In all the cases, the study of the Jacobian Matrix of the system at (p^*, q^*) gives the asymptotic stability of the unique equilibrium point. The Jacobian Matrix is given by

$$A(p^*) = \begin{pmatrix} -U_0\gamma'(p^*) & \kappa \\ \beta'(p^*)W(p) + \beta(p)W'(p) & -\kappa - \beta(p^*) \end{pmatrix} \tag{46}$$

so that for $p^* \in [0, p_h + \varepsilon)$,

$$\begin{aligned} \mathrm{Tr}(A) &= -\kappa - \beta(p^*) - U_0\gamma'(p^*) < 0, \\ \mathrm{Det}(A) &= U_0\gamma'(p^*)(\kappa + \beta(p^*)) - \kappa\beta'(p^*)W(p^*) - \kappa\beta(p^*)W'(p^*) > 0, \end{aligned} \tag{47}$$

using $W'(p^*) < 0$ and $\beta(p^*) > 0$. □

5 Conclusions and Perspectives

In this paper, we have developed a novel integro-PDE modeling approach to describe MT dynamic instability. Using parameter values calibrated from experiment or taken from the literature, we are able to simulate MT dynamics that are consistent with experiment. Further, through parameter variation, we are able to describe possible mechanisms for how destabilizing MTAs, like vinblastine, work to alter MT dynamics. In the future, it would be interesting to investigate alternate mechanisms for how MTAs alter MT dynamics, as well as how stabilizing drugs can work to alter MT dynamics. Unlike the destabilizing vinca alkaloids, stabilizing drugs like those from the taxane family bind poorly to free tubulin. Instead, they bind with high affinity to tubulin along the length of a MT (Jordan and Wilson 2004; Mohan et al. 2013), increasing the rescue frequency by stabilizing the MT lattice. At moderate to high doses, these drugs promote MT polymerization, resulting in a reduced numbers of catastrophe events and high polymerized tubulin concentrations (Mohan et al. 2013; Zhou and Giannakakou 2005).

In addition to understanding how MTAs alter normal MT dynamics, it would be useful to consider ways to extend our model in such a way as to produce stable limit cycles (or oscillations that persist for longer periods of time). This is one of the limitations of our model, as we currently are only able to sustain oscillations for short time periods. However, as this is a population-level model, this does not mean that oscillations do not exist at the microscopic level. One reason for why our model behaves in this way (does not sustain oscillations) is that we assume MT shortening events occur at the time when the hydrolysis rate and the growth rate are equal, thus we are simplifying what is happening in real systems. In particular, in real systems, MTs grow through the addition of GTP-tubulin. Once GTP-tubulin is incorporated into the MT, it is hydrolyzed to lower energy GDP-tubulin, creating a distinct GTP region at the front of a MT (the GTP-cap region). When the hydrolysis rate is larger than the

growth rate, the MT cap (which we do not account for in this model) shortens. Once it disappears, then a shortening event occurs. In future work, we could account for this by incorporating a time delay at the moment in time when the hydrolysis rate becomes greater than the MT growth rate. However, this would greatly increase the complexity of our model analysis, and is beyond the scope of this paper. The understanding of relaxation toward equilibrium of such systems is also a topic of interest and a future mathematical study will be carried out in that direction.

Acknowledgements The program is funded thanks to the support of the A*MIDEX Project (No. ANR-11-IDEX-0001-02) funded by the "Investissements d'Avenir" French Government program, managed by the French National Research Agency (ANR), and the support INSERM Plan cancer No. PC201418. D.W. was supported by the programs cited above through a post-doc funding, F.H. and M.T. were partially supported by the programs cited above. We thank Saulo de Matos Silva for his careful reading and comments, in particular for a significant improvement of proofs in Section 4.6. We thank the anonymous referees for their helpful suggestions.

Appendix: Advantages of Our Modeling Approach Over Existing Ones

Here, we illustrate a comparison between the model described here and the model of White et al. (2017). Both models describe MT dynamics in terms of simple advective growth, and incorporate a fragmentation-type term for MT shortening. The model (White et al. 2017) further incorporates an advection term to describe the growth and shortening of the MT cap region, as well as a system of ODEs to describe the binding/unbinding of end-binding proteins (EBs) to the cap.

Figure 10 describes the long-term dynamics of the "full" model of White et al. (2017) (left) and the "mini" model described in this paper (right). From this figure, it is clear that the long-term (averaged) tubulin concentrations are very similar. In particular, we make a comparison of the mean tubulin concentrations after t = 3 minutes (when the concentrations (roughly) oscillate about a mean). The steady-state values

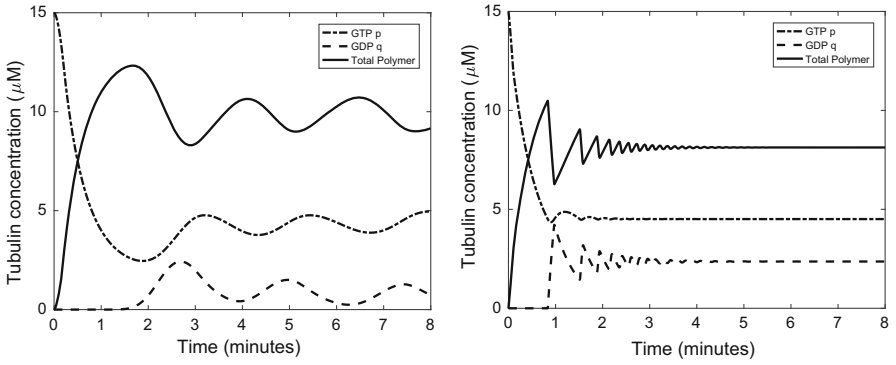

Fig. 10 Left: Full model results from simulation of model in White et al. (2017). Parameters are: $\alpha = 2$, $\gamma^{\mathrm{h}} = 5$, $\beta_\infty = 20$, $x_0 = 4$, $\mu = 5.9 \times 10^3$, $m = 2$, $x_{\min} = 0.5$, $\kappa = 2$, $p_{\mathrm{c}} = 2$, $p_{\mathrm{N}} = 12$, $p_0 = 15$, $\lambda = 0.136$. Right: Simplified model of this paper. Parameters are (units given in Table 1): $\alpha = 2$, $\gamma^{\mathrm{h}} = 5$, $\beta_\infty = 20$, $x_0 = 2$, $\mu = 0.1$, $m = 2$, $x_{\min} = 0.8$, $\kappa = 2$, $p_{\mathrm{c}} = 2$, $p_{\mathrm{N}} = 12$, $p_0 = 15$

Table 2 Table of long-term tubulin concentrations

Model	Total polymer (μM)	GTP-tubulin (μM)	GDP-tubulin (μM)
Full model (White et al. 2017)	9.73	4.35	0.91
Mini model	8.13	4.50	2.36

(calculated numerically) are recorded in Table 2. Here, all model parameters used in the simulation of the "mini" model are the same as those for the "full" model in White et al. (2017), where the full model also has a few extra parameters—all parameter values are recorded in the figure caption.

In the full model of White et al. (2017), we incorporate a compartment for shrinking MTs. In particular, MTs that undergo fragmentation (a catastrophe) do so in a separate shrinking compartment. From there, MTs that undergo fragmentation are completely depolymerized into free GDP-tubulin. For our mini model, both growth and fragmentation are described by a single equation. That is, there is no separate equation to describe MT shortening. Thus, the slight differences in concentrations could be due to the fact that, in the full model, as a MT shortens, polymerized GDP-tubulin remains in the shortening compartment for some period of time before entering the free GDP-tubulin compartment. Also, in the full model, the shortening compartment has a term for *rescue*, where some of the MTs that are shrinking enter back into the growing compartment.

References

Bayley P, Schilstra M, Martin S (1989) A simple formulation of microtubule dynamics: quantitative implications of the dynamic instability of microtubule populations in vivo and in vitro. J Cell Sci 93:241–254

Calvez V, Lenuzza N, Doumic M, Deslys J-P, Mouthon F, Perthame B (2010) Prion dynamics with size dependency-strain phenomena. J Biol Dyn 4(1):28–42

Desai A, Mitchison T (1997) Microtubule polymerization dynamics. Ann Rev Cell Dev Biol 13:83–117

Dhamodharan R, Jordan M, Thrower D, Wilson L, Wadsworth P (1995) Vinblastine suppresses dynamics of individual microtubules in living interphase cells. Mol Biol Cell 6:1215–1229

Dimitrov A, Quesnoit M, Moutel S, Cantaloube I, Pous C, Perez F (2008) Detection of gtp-tubulin conformation in vivo reveals a role for gtp remnants in microtubule rescues. Science 322(5906):1353–1356

Dogterom M, Leibler S (1993) Physical aspects of the growth and regulation of microtubule structures. Phys Rev Lett 70:1347–1350

Escobedo M, Mischler S, Rodriguez Ricard M (2005) On self-similarity and stationary problem for fragmentation and coagulation models. Ann Inst H Poincaré Anal Non Linéaire 22(1):99–125

Flyvbjerg H, Holy T, Leibler S (1996) Microtubule dynamics: caps, catastrophes, and coupled hydrolysis. Phys Rev Lett E 54:5538–5560

Gardner MK, Zanic M, Howard J (2013) Microtubule catastrophe and rescue. Curr Opin Cell Biol 25(1):14–22

Greer M, Pujo-Menjouet L, Webb G (2006) A mathematical analysis of the dynamics of prion proliferation. J Theor Biol 242(3):598–606

Hill T, Chen Y (2002) Phase changes at the end of a microtubule with a gtp cap. PNAS 81(18):5772–5776

Hinow P, Rezania V, Tuszynski J (2009) Continuous model for microtubule dynamics with catastrophe, rescue, and nucleation processes. Phys Rev E 80:031904. https://doi.org/10.1103/PhysRevE.80.031904

Jordan M, Wilson L (2004) Microtubules as a target for anticancer drugs. Nat Rev 4:253–258

Kirschner M, Mitchison K (1984) Dynamic instability of microtubule growth. Nature 312:237–242

Laurençot P, Walker C (2007) Well-posedness for a model of prion proliferation dynamics. J Evol Equ 7(2):241–264
Lodish H, Berk A, Zipursky S, Matsudaira P, Baltimore D, Darnell J (2000) Molecular cell biology, 4th edn. W. H. Freeman and Company, New York
Maly I (2002) Diffusion approximation of the stochastic process of microtubule assembly. Bull Math Biol 64:213–238
Margolin G, Gregoretti I, Cickovski T, Li C, Shi W, Alber M, Goodson H (2012) The mechanisms of a microtubule catastrophe and rescue: implications from analysis of a dimer-scale computational model. Mol Biol Cell 23:642–656
Margolin G, Gregoretti I, Goodson H, Alber M (2006) Analysis of a mesoscopic stochastic model of microtubule dynamic instability. Phys Rev E 74:041920
Mohan R, Katruha E, Doodhi H, Smal I, Meijering E, Kapitein LC, Steinmetz M, Akhmanova A (2013) End-binding proteins sensitize microtubules to the action of microtubule-targeting agents. PNAS 110(20):8900–8905
Mukhtar E, Mustafa Adhami V, Mukhtar H (2014) Targeting microtubules by natural agents for cancer therapy. Mol Cancer Ther 93:275–284
Perthame B (2007) Transport equations in biology. Frontiers in mathematics. Birkhäuser Verlag, Basel
Perthame B (2015) Parabolic equations in biology. Lecture notes on mathematical modelling in the life sciences. Springer, Cham (Growth, reaction, movement and diffusion)
Sept D, Limbach H, Bolterauer H, Tuszynski J (1999) A chemical kinetics model for microtubule oscillations. J Theor Biol 197:77–88
Simonett G, Walker C (2006) On the solvability of a mathematical model for prion proliferation. J Math Anal Appl 324(1):580–603
Wade R (2009) On and around microtubules: an overview. Mol Biotechnol 43:177–191
Walker C (2007) Prion proliferation with unbounded polymerization rates. In: Proceedings of the sixth Mississippi State–UBA conference on differential equations and computational simulations, vol 15 of Electronic Journal of Differential Equations. Southwest Texas State University, San Marcos, TX, pp 387–397
Walker R, O'Brien E, Pryer N, Soboeiro M, Voter W, Erickson H, Salmon E (1988) Dynamic instability of individual microtubules analyzed by video light microscopy: rate constants and transition frequencies. J Cell Biol 107:1437–1448
White D, de Vries G, Dawes A (2014) Microtubule patterning in the presence of stationary motor distributions. Bull Math Biol 76(8):1917–1940
White D, de Vries G, Martin J, Dawes A (2015) Microtubule patterning in the presence of moving motor proteins. J Theor Biol 382:81–89
White D, Hubert F, Honoré S (2017) Exploring the effect of end-binding proteins and microtubule targeting chemotherapy drugs on microtubule dynamic instability. J Theor Biol 429:18–34
Zauderer E (2006) Partial differential equations of applied mathematics, 3rd edn. Wiley, New Jersey
Zhou J, Giannakakou P (2005) Targeting microtubules for cancer chemotherapy. Curr Med Chem 5:65–71

Affiliations

Stéphane Honoré[1,2] · Florence Hubert[3] · Magali Tournus[3] · Diana White[4]

Stéphane Honoré
stephane.honore@univ-amu.fr; stephane.honore@ap-hm.fr

Florence Hubert
florence.hubert@univ-amu.fr

Magali Tournus
magali.tournus@centrale-marseille.fr

[1] CNRS, INP, Inst Neurophysiopathol, Faculté de Pharmacie de Marseille, Aix Marseille University, 13385 Marseille, France

2 Service pharmacie, CHU Hôpital de La Timone, APHM, Marseille, France

3 CNRS, Centrale Marseille, I2M, Aix Marseille University, Marseille, France

4 Department of Mathematics, Clarkson University, Potsdam, NY, USA